2015

Fracture Behavior of Silica- and Rubber-Nanoparticle-Toughed Epoxies

Amelia Labak
Lehigh University

Fracture Behavior of Silica- and Rubber-Nanoparticle-Toughed Epoxies

by

Amelia K. Labak

A Thesis

Presented to the Graduate and Research Committee

Of Lehigh University

In Candidacy for the Degree of

Master of Science

in

Materials Science and Engineering

Lehigh University

December 2014

CERTIFICATE OF APPROVAL

This thesis is accepted and approved in partial fulfillment of the requirements for the Master of Science in Materials Science and Engineering.

_____
Date

_____
Raymond A. Pearson
Thesis Advisor

_____
Helen M. Chan
Chairperson of Department

ACKNOWLEDGEMENTS

I would like to thank the Semiconductor Research Corporation (SRC) for funding this work through Task Number 2251.001. Additionally I would like to thank Dow Chemical, Potters Industries, and Arkema for supplying the materials that were used in this study.

I would also like to thank everyone at Lehigh University for their help and guidance. Dr. Raymond Pearson and the other members of his research group were irreplaceable for their assistance. Mike Rex and Bill Mushock are greatly appreciated for their help in technical support and training. And a very sincere thank you to everyone else in Whitaker Laboratory who helped to support my work.

Finally I would like to thank my family and friends for their continual support through this work. It means more than I can say.

TABLE OF CONTENTS

LIST OF TABLES

LIST OF FIGURES

ABSTRACT

Particle-toughened crosslinked epoxies are popular materials for a variety of applications, including the microelectronics industry. For this application, the properties of these materials, such as a high fracture toughness and a low coefficient of thermal expansion, are highly appealing. In order to achieve these properties, inorganic particles are often added into the matrix. For this study, both inorganic and organic particles-toughened epoxies are investigated in the hopes of finding an optimized system.

In particular, in this study, micron-sized silica and nano-sized rubbery block copolymers are added to an amine-cured epoxy matrix. A series of rubber-only and silica-only systems are investigated for their contribution to the fracture toughness. Then, a series of hybrid systems are investigated.

The hypothesis is that the rubber will contribute toughness through rubber particle cavitation and matrix void growth and the silica will contribute toughness through crack pinning and bridging and particle debonding. In the hybrid systems, these mechanisms will take place at a different scale. Therefore, the nanoscale mechanisms of the rubber will be able to function at the same time as the micron sized mechanisms of the silica and the resultant toughness will be synergistically higher.

The results from this study show an interesting contribution from the rubber particles both in the rubber-only systems and the hybrid system. Ultimately, there was a marked increase in the fracture toughness of the hybrid systems, although not synergistic. This increase indicates that it would be possible to create an optimized hybrid system from the combined addition of these particles.

1 INTRODUCTION

1.1 Motivation

In the 1960s, IBM introduced the Controlled Collapse Chip Connection (C4) technology to the microelectronic industry. This technology, which is now better-known as flip-chip technology, is comprised of a silicon chip that is adhered to a substrate by solder bumps and an underfill resin, as seen in Figure 1. Flip-chip devices have been found to be beneficial due to the high I-O densities, short interconnects, high throughput, improved heat dissipation, and many other factors. The purpose of the underfill resin in this package is to reduce the strain experienced in the solder joints during thermal cycling, and thus improve the lifetime by as much as 100 times [1].

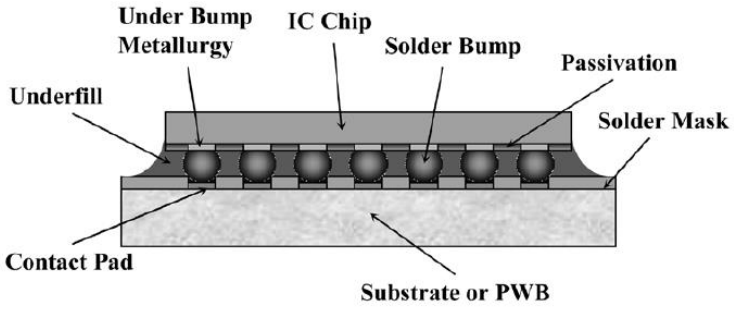

Figure 1. Schematic of general configuration of a C4 device [1].

In order improve the lifetime to this extent, it is important to optimize various material properties. Some of the properties of the underfill resin that are important for this application are the coefficient of thermal expansion (CTE), the elastic modulus, the adhesion between both the die and the substrate surfaces, and the fracture toughness. The CTE and elastic modulus play a large role in the magnitude of thermo-mechanical stresses that the package will experience. Table 1 lists the material properties for various commercial underfill resins along with other components of a flip-chip package. Of

particular note is the low CTE of the underfill resin, much lower than that of an unfilled epoxy. This low CTE was achieved by the addition of silica fillers. The goal of the reduced CTE is to lower the resulting stresses that the flip-chip package would experience due to the mismatch of CTE between the silicon chip and substrate [2]. Often, in commercial applications, 65-75 wt% of silica is added in order to achieve this effect [3].

Table 1. Material properties for various components of flip-chip packages [2].

Materials	**Elastic Modulus (GPa)**	**CTE (ppm/°C)**	**Thermal Conductivity (W/m-K)**
Silicon	112	4.1	136
Underfill A	3.6	50	X
Underfill B	3.1	35	X
Underfill C	5	29	X
Underfill D	11	23	X
Thermally conductive adhesive	11	23	3.14
Flex substrate	4.1	20	X
Solder	16	25	51
Copper	123	17	390
DCB AIN	>600	7	180

Even with the efforts to reduce the CTE of the underfill resin to lower thermo-mechanical stresses in flip-chip packages, the formation and propagation of a crack in the underfill or at the chip passivation underfill interface can occur. Therefore, there is the additional requirement of increased fracture toughness for the underfill resin. By increasing the fracture toughness, without any degradation of other material properties, crack propagation can be reduced and the lifetime of the package can be increased [1]. This increase in fracture toughness for brittle epoxies is often achieved by the addition of either soft or hard particles. The following section provides an overview of these systems as they relate to the interest of this application.

1.2 Background

There are various approaches taken to improve the material properties of a brittle epoxy resin. The approaches that will be discussed here are the addition of rubber and/or silica particles to the epoxy matrix. As mentioned above, silica particles are already used in commercial underfill resins, mainly for their ability to reduce the CTE. Silica particles implement additional benefits that will be discussed. Rubber-toughened epoxies, on the other hand, lead to an undesired increase in the CTE. However, it is possible that the increase in the fracture toughness as a result of these particles can outweigh the detrimental effects on the CTE, especially in a hybrid epoxy silica and rubber composite. This section will discuss some of the previous work conducted in these areas.

1.2.1 Epoxy Matrix

An unmodified epoxy network is often described as having a high glass transition temperature and being brittle. Of course, these, and other properties, vary depending on the system. However, in general this is a good simplification. In order to toughen the material, and make it more resistant to fracture, particles are often added into the matrix. For this composite to function, the matrix itself needs to be "toughenable", meaning that it responds positively to the addition of toughening particles.

The major factor for toughenability is crosslink density, which can also be expressed as the molecular weight between crosslinks. It is important to note that the functionality of the curing agents has been shown to play a lesser role than the crosslink density of the matrix [4]. The cure schedule can also influence the toughenability of the matrix, albeit by influencing the rubber particle size distribution for some systems [7, 8].

The toughness of epoxy resins is a function of the crosslink density. An example of the effect of crosslink density on toughness can be seen in Figure 2. In addition to the lower crosslink density materials, or materials with a higher molecular weight between crosslinks, being more inherently tough, they were more effective than the highly crosslinked systems in a rubber-toughened system [5, 6]. These results show that the crosslink density is important for the ability of the particles to impart toughness. If the system is too highly crosslinked, it will be more difficult for the particles to promote matrix shear yielding, leading to a negligible increase in the fracture toughness. Therefore, it has been concluded that lightly crosslinked epoxies are ideal systems for toughening.

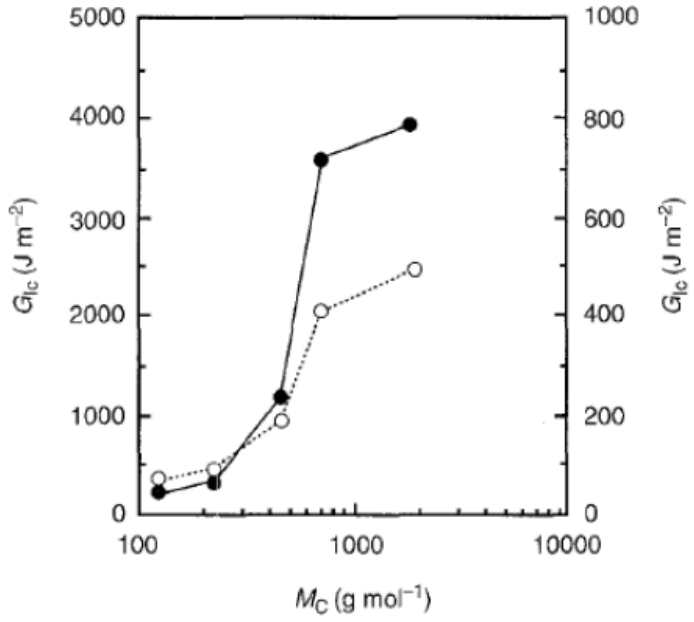

Figure 2. Effect of molecular weight between crosslinks on the toughenability of a rubber-toughened system. Neat resins: unfilled point corresponding to right axis; modified resins: filled points corresponding to left axis. [5]

The effect of the cure schedule on the toughenability of the system has also been studied. One study found that a shorter cure at a higher temperature led to a material that had a higher inherent toughness and was more effective with the addition of rubber

toughening particles [7]. Another study observed the effects of the curing agents and cure schedule on the morphology of carboxyl-terminated butadiene-acrylonitrile (CTBN) in an aromatic diamine cured diglycidyl ether of bisphenol A (DGEBA). In this study it was found that varying the curing agents led to morphological and particle size differences. Varying the cure temperature did not cause any consistent trends in varying the particle size or morphology, however, it can be seen in Figure 3 that the cure temperature did play a role in the particle formation [8]. These studies show that the cure kinetics of the epoxy system play a large role on the matrix toughness and the particle contributions in composite systems.

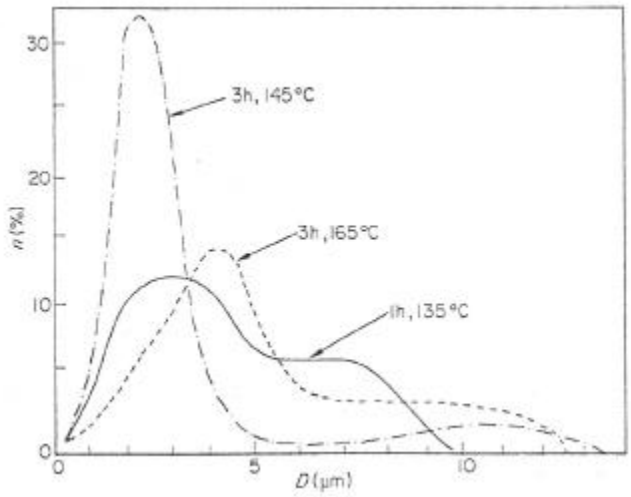

Figure 3. Particle diameter distribution of a rubber-modified system with different cure cycles. [8]

From these conclusions, it is clear that it is imperative to maintain a consistent crosslink density and cure schedule if the effect of the particles is to be isolated. One system which creates a model underfill resin and has been previously studied is DGEBA cured with 1,3-pheylenediamine (mPDA) and aniline [4, 8, 10]. A study conducted by Crawford and Lesser investigated the effect of various curing agents, and thus crosslink

functionality, crosslink density, and chain stiffness, on the resulting characteristics. One of the analyzed systems was cured with mPDA and aniline and the neat resin characteristics are presented [9]. It was seen from these studies that this system creates a toughenable system with a low crosslink density which can be employed in silica- or rubber-toughened systems.

1.2.2Rubber-Toughened Systems

In the late 1960s the technology of modification of an epoxy matrix with rubber particles was discovered. The goal of this initial invention was to improve the fracture toughness of the material [11]. This section will give a brief overview of the discoveries in this field since their inception.

1.2.2.1 Types of Rubber Particles

In general, matrices are thought of as being rubber-toughened if they are comprised of two phases. The second phase, the rubber particles, is dispersed throughout the brittle epoxy matrix and affects the resultant material properties. There are multiple ways in which to accomplish this two-phase system. One possible method is through added a liquid rubber which is initially miscible, but which reacts during the epoxy cure to phase separate. A common example of liquid rubber is a random copolymer, carboxyl terminated butadiene acrylonitrile (CTBN) that has been extensively studied and documented [6, 12-15]. Another method that has been studied is the addition of a preformed rubber particle, which will remain a separate phase the entire time and has a preset shape and size. A common example of this is a core-shell particle, another rubber particle type that has been extensively researched [10, 16].

Recently, a new option has been proposed to rubber toughen a material - the use of self-assembling block copolymers (BCPs). Similar to CTBN, these BCPs phase separate into distinct rubber morphologies during the cure process. The resulting morphology of this assembly depends on a variety of factors including the block length and composition, the interactions between all of the components, and the volume percent of the particles [17]. Unlike CTBN, the driving force behind the phase separation is not the reduced solubility of the rubber component during cure. The block copolymers are comprised of a block that is miscible in the epoxy matrix and one block that is not [18]. There are multiple ways in which BCPs can form in this manner: (1) those which react in uncured epoxy through an epoxy-miscible, and -immiscible block, (2) those where both blocks are initially miscible, but one phase separates through a reaction during cure, and (3) those that have an epoxy-miscible block which is reactive towards the epoxy or curing agent [21].

A schematic of the various morphologies that a BCP can form can be seen in Figure 4. Research has been conducted in order to determine the parameters which determine the resultant morphology and the effect of that morphology on the material properties [17-21]. Many of the studies of BCPs have dealt with the spherical micelle morphology due to difficulty of creating wormlike micelles. In order to stabilize wormlike micelles, a very narrow composition range is needed [17]. One study determined that the miscibility between the epoxy-miscible block and the epoxy and curing agents played a large role on the resultant morphology [20]. In general, for the resultant properties, it has been seen that the wormlike micelles were able to transfer the most toughness to the epoxy

matrix. Additionally, both wormlike and spherical micelles led to an increase in the glass transition temperature of the component [21].

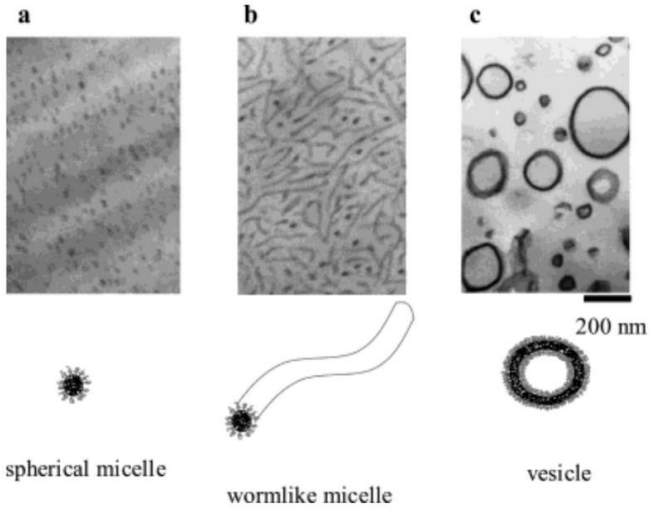

Figure 4. Possible resultant morphologies from BCPs [19].

1.2.2.2 Rubber Toughening Mechanisms

The study of the mechanisms that allow the rubber particles to impart toughness to the matrix is an important step in order to determine the optimal formulation. There are multiple mechanisms which have been introduced and investigated as major contributors to the toughness of the material. The major three of these mechanisms, particle cavitation and void growth, shear banding, and crack bridging, can be seen schematically in Figure 5. The simplest explanation of crack bridging is having damaged rubber particles in the crack path, where energy is taken from the crack to deform these particles [11]. Kunz-Douglass et al. developed a model where the dissipation of the energy was achieved through the crack bridging by stretching rubber particles [23]. Since the creation of this model it has been determined that the energy dissipation from this method is minor and the focus has been shifted to study process zone mechanisms.

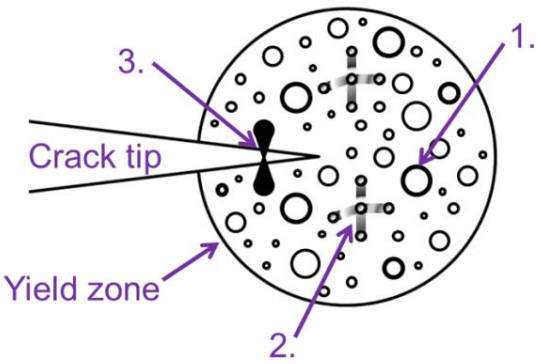

Figure 5. Schematic representation of the major toughening mechanisms: (1) rubber particle cavitation and matrix void growth, (2) matrix shear banding, and (3) crack bridging by the rubber particle [22].

The second type of toughening mechanisms work in a process zone, not directly at the crack tip, as is shown by the circle region surrounding the crack tip in Figure 5. These mechanisms include particle cavitation and matrix shear band growth. The combination of these effects leads to a large amount of plasticity and stress whitening which was not explained by the model by Kunz-Douglass et al. Huang and Kinloch created a model including these mechanisms in a plane-strain situation [22, 24]. This model has been found to fit relatively well with experimental data [18, 25] indicating that these mechanisms play a major role in the toughening of the epoxy matrix. The reason these are thought to function is that the particle cavitation leads to a reduction in the hydrostatic tension and initiates the growth of shear bands [27].

1.2.2.3 Resultant Rubber-Toughened Material

It is difficult to briefly summarize the effects of rubber tougheners on an epoxy system, therefore, this section will overview the reasons this material is interesting for research and the potential difficulties. As mentioned and discussed above, the major interest of the rubber-toughened system is the increase in fracture toughness. In general, it is found that rubber increases the fracture toughness below a specific loading

concentration. Figure 6 shows an example of the drop in fracture energy when the loading is higher than 20 phr rubber [26]. As can be seen from this figure and as reported elsewhere, the addition of rubber is capable of up to tenfold increases in the fracture toughness. Another note for this figure is that it has been seen that the addition of above 30 phr rubber has led to a phase inversion with the matrix [27].

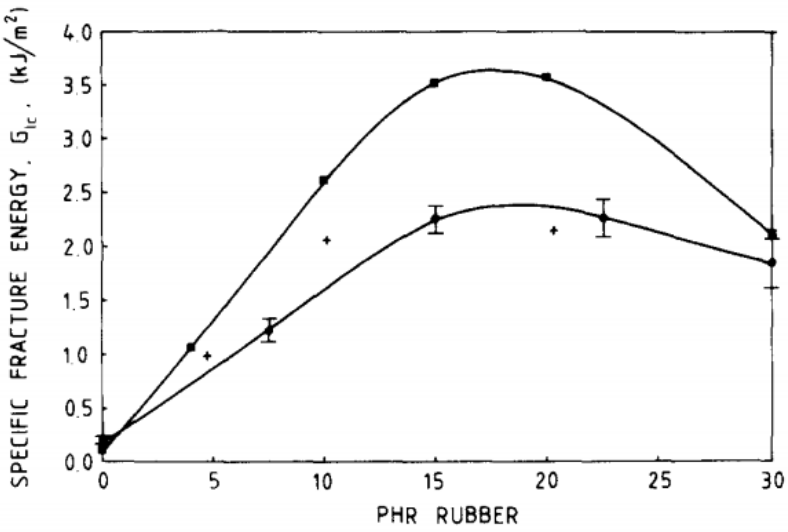

Figure 6. Effect of rubber content on specific fracture energy. (+) Yee and Pearson, (■) Bascom et al, (●) Garg and Mai [26].

In addition to the effect of the filler concentration, the filler particle size plays a role in the benefit of the particles for fracture toughness. The reason behind the importance of this parameter is the role that the particles can play in the process zone. If the rubber particles are larger than the process zone, the toughness they can impart to the system is reduced. To this effect, Pearson and Yee discovered that the particles 0.1 mm in diameter were able to increase the toughness more than a 100 mm particle [28]. The addition of nano-sized rubber fillers has also been seen to increase the fracture toughness [17, 20, 21]. A model has been created in order to attempt to quantify this effect of particle size on the particle cavitation mechanism, and thus the toughness of the material [29].

There are some negative effects of the addition of rubber tougheners, which vary in importance, depending on the application. These negative effects include a reduction in stiffness, a decrease in the glass transition temperature, a reduction in the yield strength, and an increase in the CTE [26]. Changes in such properties are also functions of the rubber particle size and filler concentration. One study found that the rubber particle size did not play a role on the yield behavior of the material [14]. However, the rubber content has been found to play a role in all of these characteristics. If it is important to maintain the initial mechanical properties of the epoxy system, the inclusion of silica particles can be used to maintain these properties, but also include the toughening benefits of the rubber particles, as will be discussed in future sections.

1.2.3 Silica-Toughened Systems

The addition of silica to a brittle epoxy matrix is a documented method to improve the mechanical properties [30-39]. When the silica particles are added, there is a slight increase in the fracture toughness, without a decrease in the modulus. Additionally, the CTE is decreased with the addition of silica, a feature that is often desired for the end application [30]. The effect of the silica particle depends on a variety of factors that will be briefly discussed below.

1.2.3.1 Types of Silica Particles

One of the parameters which plays a role on the efficacy of the silica filler content is the particle shape. One study by Ahmad et al. investigated the effect of four different silica shapes: angular, cubical, mineral, and irregular [31]. In this study, they found that there was not much difference between the various shapes, except for the irregular shaped particles, which showed a much lower flexural strength. Their theory was that the low

strength in the irregular shape was due to poor interfacial bonding and stress concentrators at the tips of the particle. What should be determined from this study is that an irregular shape silica particle should be avoided.

Another parameter, which was touched upon in the discussion of particle shape is the particle-matrix adhesion. One study looked into the effect of particle-matrix adhesion and determined that while it is important for the particles to be partially included, a relatively poor particle-matrix adhesion actually leads to higher fracture toughness. The degree of debonding, which is a large toughening mechanism for silica-toughened materials, is highly dependent on the surface treatment or particle-matrix adhesion [32-33]. Additionally, it is thought that with a poor particle-matrix adhesion, the size of the diffuse shear zone is increased. This would lead to possible further interactions with silica particles, slowing the crack [34].

In addition, the size of the silica particles plays a role in the effect of the filler on the epoxy matrix. Both micron and nano-sized silica particles have been investigated in order to determine the optimum content and loading for mechanical properties. It has been seen in nano-sized particles that there is not a significant effect of particle size on the fracture toughness [30, 37]. In the micron range, there is a slight increase in the fracture toughness seen with the decrease in particle size. This improvement is attributed to the increase in the amount of particles that comprise a specific loading when the size is decreased. Additionally, the increase in toughness from the micron range to the nano-range is thought to be due to an increased impact of the particle-matrix interface. With nanoparticles, the surface area of the particles drastically increases, causing that property to gain importance [36].

One final parameter that will be mentioned is simply the filler concentration. Varied amounts of silica particles vary the properties of the epoxy composites. It has been seen that increasing amounts of silica particles leads to increases in the fracture toughness, Young's modulus, and flexural strength and a decrease in the CTE [31, 33, 35, 36]. One note is that while an increase in fracture toughness is found, it is a general trend that it plateaus around 20 or 30 vol%. It has been noted that the change in these properties could be attributed to the change in the crack propagation. With higher volume percent of silica particles, the crack would have to travel around the particles in order to propagate. Therefore, the increase of particles in the process zone increases the energy required for the crack to debond or move around those particles [34]. Another note about the effect of filler concentration is that care should be taken in terms of agglomeration. If particle agglomeration occurs it is possible that the effective particle size or the interparticle distance will vary, which has been seen to have a detrimental effect on the fracture toughness [38].

1.2.3.2 Silica Toughening Mechanisms

Multiple toughening mechanisms have been proposed to explain the increase in toughness that is seen in epoxy-silica composites. These mechanisms include: crack-tip pinning, crack path deflection, particle debonding, matrix shear banding, and particle bridging. The extent of each of these mechanisms on the composite is a function of the previously described parameters, however, what are generally thought of as the most important mechanisms will be presented here. The three mechanisms that will be focused on are crack pinning, debonding, and matrix shear banding.

The idea of crack pinning is that the motion of the crack is impeded by the presence of the particle in the matrix. This can be seen by crack bowing between two particles that are well-adhered to the matrix. If the particles are fully able to arrest the motion of the crack, it will remain bowed between the particles. This mechanism can be seen in Figure 7. If the particle is not as well-adhered to arrest the crack, oftentimes the crack will be seen to deflect, moving from one weak interface to the next [30]. Crack pinning has been observed regardless of particle size, although there is some debate as to whether nanosilica particles are large enough to cause this mechanism. Johnsen et al have stated that for crack pinning to be a valid mechanism, the particles must be larger than the crack-opening displacement [39].

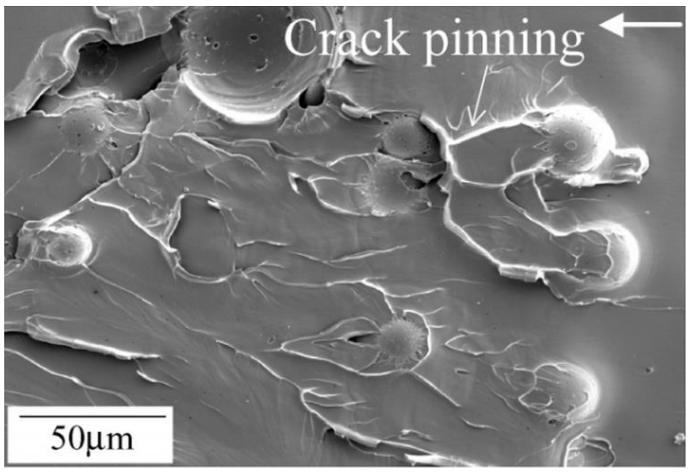

Figure 7. SEM image showing crack pinning in a silica-epoxy composite [33].

Another toughening mechanism that can contribute large amounts of fracture toughness is particle debonding. In this mechanism, some of the energy from the crack is dispersed in order to debond the particles from the matrix. It is normally thought that the energy used to debond the particle is small compared to the energy used to create the subsequent matrix void growth [39]. This matrix dilatation is possible due to the decrease in the triaxiality of the matrix that occurs after the particle debonds [32]. This particle

debonding and subsequent void growth can be seen in Figure 8. One note about debonding is that there is a current investigation into the amount of silica particles that debond from the matrix, as this will have a large effect on the toughness this mechanism provides. One study has seen that 14.3% of the particles debond, a relatively low number considering the amount of toughness they add to the system [37].

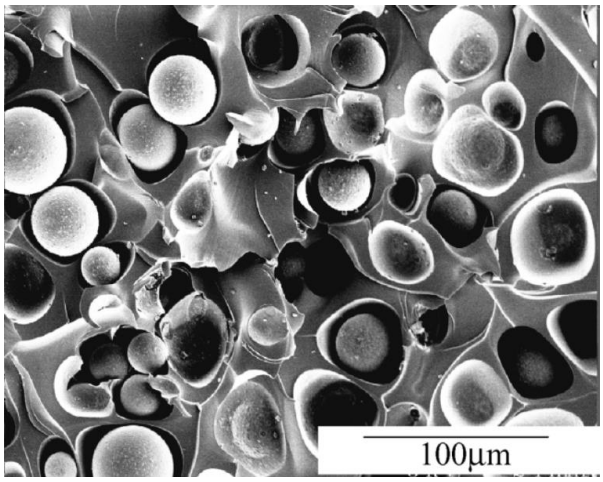

Figure 8. SEM image showing particle debonding in a silica-epoxy composite [32].

1.2.3.3 Resultant Silica-Toughened Materials

As stated in Section 1.2.3.1, the properties of the silica-epoxy composite are highly dependent on the parameters of the particles involved. However, an overview of the resultant properties shows that continued research of these systems is interesting. As mentioned previously, epoxy-silica composites are seen to have improved fracture toughness, yield stress, CTE, and modulus. These beneficial properties are very interesting and might be able to provide a synergistic effect to a hybrid epoxy silica rubber composite system as will be discussed in the following section.

1.2.4 Hybrid Rubber Silica Systems

The addition of silica and rubber together to create a tougher material has been investigated for the last 20 years. The toughing benefits of each of the particles by

themselves were studied and it was hypothesized that they might have synergistic effects if combined. One of the properties that has been varied in the research of hybrid composites that has been conducted is the particle size of both the silica and the rubber particles. Initial work looked at micron sized silica and rubber particles [40-42]. Since then, the discovery of nano-sized silica particles has been introduced to the hybrid research and this formulation has been investigated [43-45].

The interest in this research is that the combination of these particles has been shown to have a synergistic effect on the fracture toughness. An example graph showing the synergistic effect can be seen in Figure 9. These studies have found that the particle size and filler concentration plays a role on the toughening that the particles are able to impart. The following section will discuss the ways in which these particles interact in order to either benefit the toughness or have minimal synergistic effects.

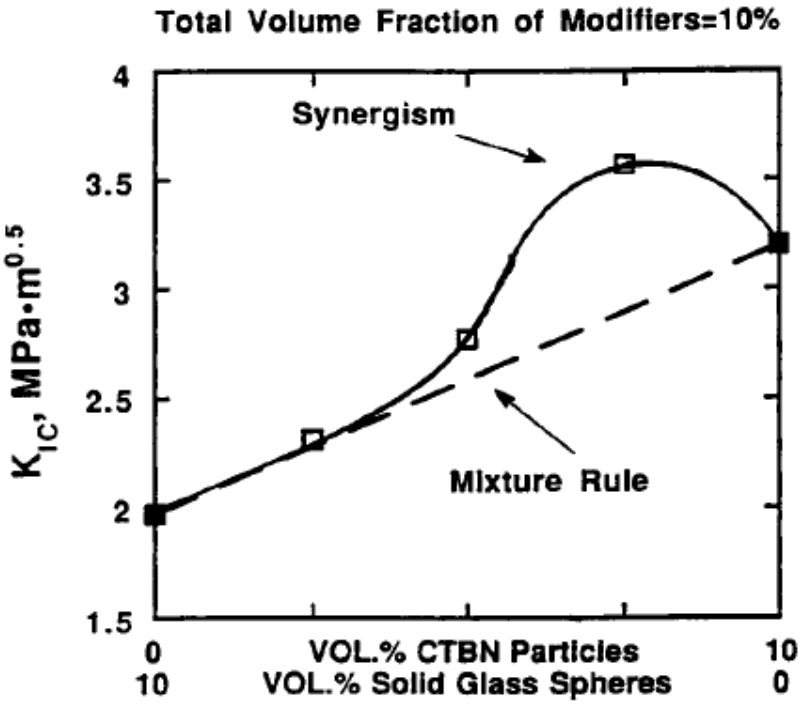

Figure 9. Synergistic toughening effect of hybrid epoxy-silica-rubber composites [40].

1.2.4.1 Hybrid Toughening Mechanisms

The toughening mechanisms for silica or rubber particles that are not in the presence of each other has been described in previous sections. However, when the particles are added into a hybrid system, a synergistic increase has been noted in some cases. This synergy means that it is not merely an additive process and the particles actually assist each other to promote toughening. In micron-sized rubber and silica hybrid systems, the reason for this synergism has been attributed to the cavitation of the rubber particles and the reduction in hydrostatic stress that results in the matrix. This reduction leads to a lower driving force for the silica particles to debond which leads to a higher efficiency in crack pinning by these particles [40]. It has also been noted that the cavitation and shear banding of the rubber particles can be increased by the local stress concentrations generated by the glass particles [41]. This increase in the matrix plasticity is also thought to contribute to crack blunting, which is only possible at yield stresses lower than 100 MPa [42]. In all, it is seen that the particles work together in multiple ways to make a tougher material.

The systems that combined nanosilica with rubber show increases due to similar toughening mechanisms. There is a presence of cavitated rubber particles and a small amount of debonding of the nanosilica particles [44]. Another study noted that with the addition of small amounts of silica nanoparticles the crack tip was blunted due to the increase matrix plasticity [43]. This study also attributed the synergistic toughening effects to the interparticle distance between the micron rubber and nanosilica. Therefore, for the hybrid systems in general, there is no new toughening mechanism seen for the particles.

However, the toughening mechanisms that were noted for the solitary tougheners are seen to be amplified by the addition of the other phase.

1.3 Objective

The preceding discussion has touched upon the ways to toughen a brittle epoxy matrix with rubber, silica, or hybrid rubber and silica additions. One lacking data point in this discussion is the creation of hybrid systems with nano-sized rubber particles and micron sized silica. The objective of this study is to elucidate this point in the hopes that it will contribute to a fuller understanding of these hybrid systems. For this study, self-assembling block copolymers will be used to create a nano-phase of rubber and will be added to a micron-sized silica system. These systems will then be investigated to determine the fracture toughness and the mechanisms which contribute to that toughness. If this system is sufficiently tough, along with a sufficiently low CTE, it will have the potential to be further studied for a role in underfill applications.

2 MATERIALS AND EXPERIMENTAL

2.1 Materials

The epoxy matrix in this study is amine cured and lightly crosslinked. This matrix serves as a model epoxy system that is capable of incorporating various fillers due to the relatively low level of crosslinking. The epoxy resin is diglyidyl ether of bisphenol A (DGEBA) with the designation of D.E.R. (Dow Epoxy Resin) 331 provided by Sigma Aldrich. This epoxy has a molecular weight of 374 g/mol. 1,3-phenylene diamine (mPDA) and aniline, provided by Acros Organics and Alfa Aesar, respectively, were used to cure the system. They were added in the stoichiometric ratio of 1 mPDA: 2 aniline: 4 epoxy to

ensure consistent crosslinking. The chemical formulations of these materials can be seen in Figure 10.

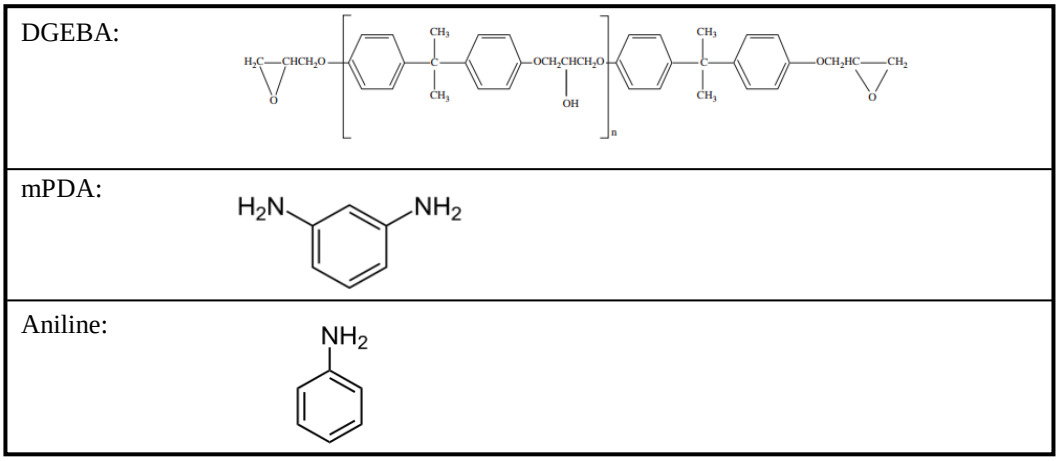

Figure 10. Chemical structures of epoxy and curing agents used in the study.

For this study, two types of fillers were added into this neat resin (NR) epoxy matrix. The first filler added was a diblock copolymer with a block of polymethyl methacrylate (PMMA) and a block of poly butyl acrylate (PBA). It was provided by Arkema, who identify this rubbery block copolymer (BCP) as nanostrength D51N. It has a molecular weight of 50,000 g/mol. The second type of filler added to the matrix, either solely or in the presence of the rubber phase, were solid glass spheres. These were provided by Potters Industries, who identify this material as EMB-10, Spheriglass solid glass spheres. These particles, with a mean diameter of 5 μm, were used as provided and were untreated, meaning there was no surface modification

The rubber was added in terms of parts per hundred rubber (phr). The silica was added in terms of volume percent (vol%). A full list of the formulations used in this system can be seen below in Table 2.

Table 2. Filler formulations used in the study.

Type	System	BCP Content (phr)	Silica Content (vol%)
NR	**Neat Resin**	0	0
BCP	**2.5 phr**	2.5	0
	5 phr	5	0
	7.5 phr	7.5	0
	10 phr	10	0
Silica	**10 vol%**	0	10
	15 vol%	0	15
	20 vol%	0	20
	30 vol%	0	30
Hybrid	**2.5 phr/20 vol%**	2.5	20
	2.5 phr/30 vol%	2.5	30
	5 phr/ 20 vol%	5	20
	5 phr/30 vol%	5	30

2.2 Formulations and Processing

2.2.1 Formulations

In order to determine the stoichiometric quantities of curing agents that needed to be added to the epoxy, calculations were conducted following Equations 2.1 and 2.2. The values for molecular weight that were input into these equations can be seen in Table 3.

Table 3. Molecular weights of components to formulate the NR.

	D.E.R. 331 Epoxy	mPDA	Aniline
Molecular Weight (g/mol)	374	110	94

$$mass_{mPDA} = mass_{epoxy} * \left(\frac{110}{4*374}\right) \qquad \textbf{(2.1)}$$

$$mass_{aniline} = mass_{epoxy} * \left(\frac{94}{4*374}\right) \qquad \textbf{(2.2)}$$

The amount of epoxy added to these equations was decided based on the size of the sample that needed to be made. The amount of epoxy ranged from 200-375g based on the amount of filler added to the NR. For example, the NR sample was made from 300g of epoxy and, by solving Equations 2.1 and 2.2, it can be found that the amount of mPDA

needed was 22.06g and the amount of aniline was 37.70g. An overview of all of the systems can be seen in Table 4.

Table 4. List of the mass formulations used for this study.

Type	System	$mass_{epoxy}$ (g)	$mass_{mPDA}$ (g)	$mass_{aniline}$ (g)	$mass_{BCP}$ (g)	$mass_{silica}$ (g)
NR	**NR**	300	22.06	37.70	0	0
BCP	**2.5 phr**	360	26.47	45.24	9	0
	5 phr	375	27.57	47.13	18.75	0
	7.5 phr	370	27.21	46.50	27.75	0
	10 phr	375	27.57	47.13	37.5	0
Silica	**10 vol%**	350	25.74	43.98	0	102.60
	15 vol%	300	22.06	37.70	0	139.67
	20 vol%	300	22.06	37.70	0	197.88
	30 vol%	200	14.71	25.13	0	226.13
Hybrid	**2.5 phr/20 vol%**	200	14.71	25.13	5	138.57
	2.5 phr/30 vol%	200	14.71	25.13	5	237.54
	5 phr/ 20 vol%	200	14.71	25.13	10	134.66
	5 phr/30 vol%	200	14.71	25.13	10	230.85

The amounts of fillers needed to create the plaques described in Table 2 were determined in a variety of ways. The BCP was added in units of parts per hundred resin (phr). An example of this is that 5 g of BCP in 100 g of epoxy resin would create a 5 phr sample. This measurement was simple as it did not take into account the curing agents. The silica was added in units of volume percent (vol%). Therefore, for this measurement it was necessary to determine the density of the cured resins ($\rho_{cured\ resin}$). This method is described in Section 2.3.1. In the silica only systems, the density of the neat resin was used. In the hybrid systems, the densities of the 2.5 phr and 5 phr systems were used. After determining these densities, the amount of silica added was found using Equation 2.3. The mass of the cured resin that is used in this equation can be found using Equation 2.4. These calculations led to the formulations that were used in this study and can be seen in Table 4.

$$mass_{silica} = \left(\frac{mass_{cured\ resin}}{\rho_{cured\ resin}*(1-vol\%\ silica)}\right) * vol\%\ silica * \rho_{silica} \quad \textbf{(2.3)}$$

$$mass_{cured\ resin} = mass_{epoxy} + mass_{mPDA} + mass_{aniline} + mass_{BCP} \quad \textbf{(2.4)}$$

2.2.2 Processing

In order to mix and process these samples it was necessary to adjust the schedule slightly. A list of all of the processes can be seen below in Table 5. The determination for the need for processing differences arose from flaws in the completed plaques. There was an issue in the plaques containing BCP of voids being present. In order to eliminate these voids, the vacuum was consistently held, other than the 5 minute initial mixing of the curing agents to the system. This problem of voids was exacerbated by the addition of silica in the hybrid system, which increased the viscosity. Therefore, for the hybrid systems it was necessary to reduce the sample size to 200g epoxy, as can be seen above in Table 4. Also, there was an issue in the plaques containing silica where settling was occurring. In order to counter this effect, the plaque was flipped every half hour for six hours. Six hours was used as it had been determined as the gel time of this epoxy system at 50°C in a previous study and it was assumed that at the viscosity at the gel point, the motion of the particles would be eliminated. The cure and post-cure schedule was taken from the work of Crawford and Lesser [9].

Table 5. List of the mixing and curing schedules for all of the systems.

System	Mixing Schedule	Cure Schedule	Post-Cure Schedule
NR	Add curing agents to epoxy 5 min. at 80°C 10 min. at 80°C under vacuum Pour into plaque	12 hours at 50°C	3 hours at 130°C
BCP only systems	Add BCP to epoxy 2 hours at 80°C 2 hours at 140°C under vacuum Cool down to 80°C under vacuum Add curing agents 5 min. at 80°C 10 min at 80°C under vacuum Pour into plaque		
Silica only systems	Add silica to epoxy 30 min. at RT 30 min. at 80 30 min. at 80°C under vacuum Add curing agents 5 min. at 80°C 10 min at 80°C under vacuum Pour into plaque	12 hours at 50°C (Flip the plaque 180° every 30 min. for the first 6 hours)	
Hybrid systems	Add BCP and silica to epoxy 2 hours at 80°C 2 hours at 140°C under vacuum Cool down to 80°C under vacuum Add curing agents 5 min. at 80°C 10 min at 80°C under vacuum Pour into plaque		

2.3 Characterization

2.3.1 Density

It was necessary to find the density of some of the cured resin systems and the silica particles in order to determine accurate volume fractions of silica for the systems. The methods used are detailed in the following two sections.

2.3.1.1 Cured Resin Density

After the samples were made, the density was found for the neat resin, 2.5 phr, and 5 phr systems. These densities were used in the calculations to determine the amount of silica needed for the hybrid systems, $\rho_{cured\ resin}$ in equation 2.3.The method used to find the density was the buoyancy method based on Archimedes' principle. The Torbal Density Analyzer Kit was used to measure the weight of a sample in air and in room temperature deionized water. This kit takes into account the change in buoyancy with water temperature, the air buoyancy, and the change in the immersion level of the hanging pan with displaced water. The user controlled error that must be watched for is air bubbles trapped on the surface of the sample. If bubbles are included, there will be a large effect on the measured density, so air bubbles must be removed from the sample.

After finding the wet weight (W_w), dry weight (W_d), and recording the temperature of the water at the time of measurement, the density of the system ($\rho_{cured\ resin}$) can be found as shown in equation 2.5. $K_{immersion}$ is a factor used to account for the interface of the sample and the water, equal to 0.99989 for the 400 ml beaker used. The density of the air (ρ_{air}) can be approximated as 0.0012 g/cm^3 by assuming the test is conducted at sea level in a 50% humidity and 20°C environment.

$$\rho_{cured\ resin} = \frac{W_d*(\rho_{water}-\rho_{air})}{K_{immersion}*(W_d-W_w)+\rho_{air}} \quad \textbf{(2.5)}$$

2.3.1.2 Filler Particle Density

Another density test that was conducted was using a pycometer in order to confirm the density of the silica particles. For this method the pycometer is weighed (m_0). Then a run was conducted where the bottle is filled only with the liquid of known density (ρ_{water}) and weighed (m_3). The bottle was then dried and the particles are added and

weighed (m_1). The bottle was then filled with a liquid of known density (ρ_{water}) and the bottle was weighed again (m_2). The density of the particles ($\rho_{particles}$) can then be determined as seen in equation 2.6.

$$\rho_{particles} = \frac{m_1 - m_0}{(m_3 - m_0) - (m_2 - m_1)} * (\rho_{water} - \rho_{air}) + \rho_{air} \qquad \textbf{(2.6)}$$

One word of caution about this test is that care must be taken to ensure that the particles are fully wetted and not agglomerated. In this study, in order to ensure that this was the case, the water was added to the particles and then ultrasonically agitated for 30 minutes. After that process it was assumed that the particles were fully wet as no agglomeration was visible, however, the water was noted to be full of particles leading to a murky visibility. When the cap of the pycometer is added, some water leaks out the top, in order to fully fill the bottle. If there were particles in that lost water, the density measurement would not be accurate. Therefore, the bottle was left for 48 hours to allow the particles to settle. After this time it was noted that the water was again clear at the top of the bottle and the top could be placed without a concern for lost particles.

2.3.2 Filler Composition

Due to the various types of particles added to the system, organic versus inorganic, it was necessary to confirm the filler composition in two different manners. These manners are detailed below.

2.3.2.1 Silica Filler Composition

The silica particles are purely inorganic, therefore the composition of the silica particles in the silica or hybrid systems can be determined with thermogravimetric analysis (TGA). The machine used for this analysis was a TA Instruments Q500 TGA. A 10-15 mg size sample of the system being tested was loaded on to a platinum sample pan.

The sample was then heated in an air environment from 25°C to 700°C at a rate of 10°C/min. At that point all of the organics, the neat resin or the neat resin and the rubber fillers, were burned off and the weight reading was purely from the silica. From this remaining weight percent of silica fillers it was possible to determine the volume percent of silica as seen in equation 2.7.

$$vol\%\ silica = \frac{wt\%\ silica / \rho_{silica}}{wt\%\ silica / \rho_{silica} + (1 - wt\%\ silica) / \rho_{cured\ resin}} * 100 \quad \textbf{(2.7)}$$

An average of two measurements was taken for the vol% silica from two opposite portions of the plaque to ensure that no settling of the silica particles had occurred. For example, one measurement was taken from the top and front of the plaque and the second was taken from the bottom and back of the plaque.

2.3.2.2. Rubber Filler Composition

The rubber filler composition was calculated based on the amount of BCP added to the system. Due to the nature of the diblock copolymer, half of the block comprises the rubber portions (PBA) of the material. The miscible block is assumed to have properties comparable to the epoxy matrix. Therefore, the volume percent of rubber was found as seen in equation 2.8, where the mass of the NR ($mass_{NR}$) is comprised of the weight of the epoxy, mPDA, and aniline. The density of PBA was taken as 1.087 g/mL.

$$vol\%\ rubber = \frac{0.5 * mass_{BCP} / \rho_{PBA}}{(0.5 * mass_{BCP} + mass_{NR}) / \rho_{NR} + 0.5 * mass_{BCP} / \rho_{PBA}} \quad \textbf{(2.8)}$$

2.3.3 Glass Transition Temperature (T_g)

The glass transition temperature (T_g) of all of the systems was determined using differential scanning calorimetry (DSC) following ASTM E-1356-08 [46]. The machine used for this method was a TA Instruments Q2000 DSC. A sample sized between 5-10 mg

was taken from each of the systems and placed in a hermetically sealed aluminum pan. These samples were then run through a heat-cool-heat cycle from 25°C to 200°C. The T_g was analyzed using the midpoint method from the second heat cycle; the first heat and cool cycles were used to remove any effects of physical aging or thermal history. An average was taken from two samples removed from various portions of the plaque to ensure consistency.

2.3.4 Coefficient of Thermal Expansion (CTE)

The coefficient of thermal expansion (CTE or α) was determined using thermomechanical analyzer (TMA) and following ASTM E831-14 [47]. The machine used for this method was a TA Instruments TMA 2940 with a macro-expansion probe. A sample was machined to 5 mm x 5 mm x 5 mm. Every side was measured to ensure that they were parallel to within 25 μm of each other. After the sample was loaded such that the center of the sample aligned with the center of the probe, the sample was run through a heat-cool-heat cycle. The initial heat-cool cycles were conducted from 25°C to 200°C at 5°C/min in order to erase any physical aging or thermal history. The second heat cycle was conducted from 25°C to 200°C at 1°C/min and was used to make measurements for the CTE below and above T_g, α_1 or α_2, respectively. An average was taken from two samples.

2.3.5 Compressive Yield Strength (σ_y)

The compressive yield strength, σ_y, was determined using ASTM D695 [48]. The samples used were machined to the size of 6 x 6 x 12 mm. The machine used for this analysis was an Instron 5567 Universal Testing Frame with a polished plate base and test head. The sample and the base and head of the machine were coated in a graphite lubricant

prior to loading in order to ensure that there was a minimal contribution from friction. Then the sample was placed so that the center was aligned with the center of the test head. The test was conducted with a crosshead speed of 1.3 mm/min and the compressive yield strength was determined by taking the maximum compressive load and dividing it by the original cross section (MPa). An average was taken from five samples.

2.3.6 Fracture Toughness (K_{IC})

The fracture toughness, K_{IC}, was determined using a single-edge- notched three point bend (SEN 3PB) following ASTM D5045 [49]. The machine used for this analysis was an Instron 5567 Universal Testing Frame with a three-point bend set-up. The sample was machined to the size of 0.5 x 3 x 0.25 inches. The center of the sample was then notched with a jeweler's saw. After this notch was made, the crack needed to be initiated. In order to ensure that the crack was atomically sharp surrounded by no plastic deformation, the razor blade was cooled in liquid nitrogen for 15 minutes before being used. Using a hammer, the razor blade was then tapped into the center of the notch to roughly 50% of the distance through the sample. The samples were then loaded onto the Instron and the three-point bend test was conducted at 1 mm/min.

After the sample fractured, the crack was analyzed in order to determine if the measurement was a valid K_{IC} value. The thickness of the sample was measured along with three points of the initial crack length (left, middle, and right). In order for the measurement to be valid, three requirements must be met. First, each of the measured crack lengths must be within 10% of the others. Inclusive in this requirement is that the shape of the crack should be visible as a stress whitened region and "penny" shaped. An example of what the crack shape should look like can be seen in Figure 11 along with a

"w" and a "half penny" crack shapes, which are undesirable. The second requirement is that the average crack length from those three measurements is between 45% and 55% of the entire sample. The third requirement is that a size criteria that ensures that the sample is in plane strain and that the un-cracked portion of the sample (the width minus the crack length) is large enough to avoid excessive plasticity [49]. This size requirement can be seen in equation 2.9, where B = thickness, W = width, a = crack length, K_Q = trial K_{IC} value, and σ_y = tensile yield stress. The tensile yield stress is calculated as 0.7 times the compressive yield stress [49].

$$B, a, (W - a) > 2.5 * \left(\frac{K_Q}{\sigma_y}\right)^2 \quad \textbf{(2.9)}$$

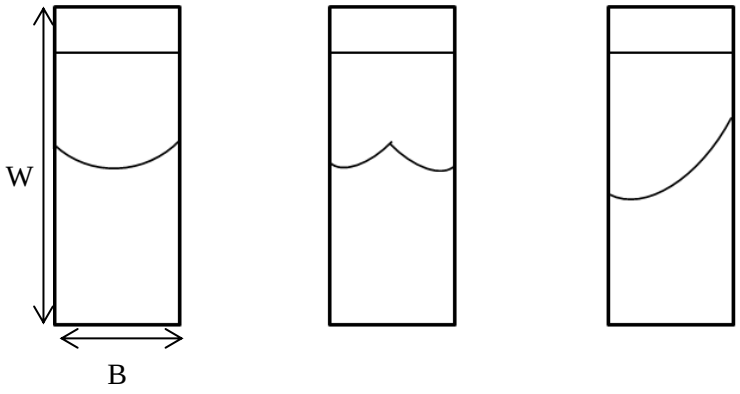

Figure 11. Schematic crack shapes, penny, w, and half penny (from left to right).

For the samples that were found to have passed the three criteria for a valid K_{IC} measurement, the K_{IC} was calculated as seen in equation 2.10. Equation 2.11 shows what f(x), the shape factor, entails. Additionally, P_Q is the maximum load, B is the specimen thickness, W is the specimen width, a is the crack length, and $x = a/W$. An average was taken from five samples.

$$K_{IC} = \left(\frac{P_Q}{B * W^{1/2}}\right) * f(x) \quad \textbf{(2.10)}$$

$$f(x) = 6x^{1/2} * \frac{[1.99 - x(1-x)(2.15 - 3.93x + 2.7x^2)]}{(1+2x)(1-x)^{3/2}} \qquad \textbf{(2.11)}$$

2.3.7 Fracture Surface and Mechanisms

In order to determine the formation of the particles in the matrix and the effect of these particles on the fracture of the sample, it is necessary to look at the system using scanning electron microscopy (SEM). The machine used for this analysis was a Hitachi 4300 low voltage SEM. The samples were placed on the 12.5 mm sample stub using carbon tape and then coated with 5 nm of iridium in order to prevent charging and sample damage. In the SEM, the stress whitened zones and the fast fracture zones of the samples were observed. From these images it was possible to determine the particle distribution and the mechanisms of fracture.

2.3.8 Plastic Zone Size

The plastic zone size was determined using transmission optical microscopy (TOM). The machine used for this analysis was a Olympus BH-2 light optical microscope. In order to determine the plastic zone, a cross-section of the crack surface from the SEN-3PB was analyzed, as depicted in Figure 12. Through an analysis of this central cross-section it is possible to see the subsurface damage of the crack tip without interference from the sample sides. These samples were sectioned approximately 0.5 inches away from the fracture surface in order to ensure no thermal effects reaches the subsurface damage. The sample is then mounted in epoxy then ground and polished through roughly half of the sample thickness (0.125 inches). The polished side is then mounted with epoxy to a glass slide. Finally, the other side is polished using petrographic means to a thickness of 100 μm ± 10 μm.

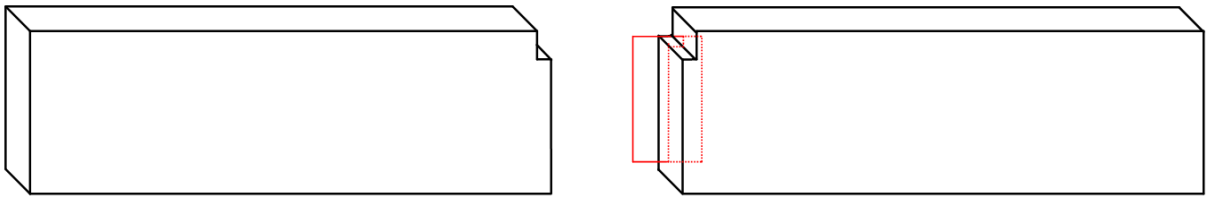

Figure 12. Fractured sample from a SEN 3PB test where the red plane depicts the plane analyzed in TOM.

The thin sample is then looked at in transmission mode on an optical microscope using both bright field and cross-polarized light. Under the bright field conditions, the surface damage, such as voiding, will scatter the light and appear dark in the micrograph. Under cross-polarized conditions, the surface damage, which creates birefringence, such as shear bands, will appear bright. A measurement is taken from the images in order to determine the size of the plastic zone, a value which helps to depict the amount of energy that was dissipated by the material.

3 RESULTS AND DISCUSSION

3.1 Results

3.1.1 Filler and Matrix Density Measurements

Using the pycometer, the density of the silica particles was determined. The found density of the particles was 2.64 g/cm^3. This measurement corresponds well with the MSDS value given for the particles of 2.6 g/cm^3, therefore, it was taken to be an accurate measurement.

Using the Torbal density kit, the densities of the neat and the 2.5 phr BCP and the 5 phr BCP modified epoxy systems were found. The density results are listed in Table 6. Note that the density of the toughened matrix did not change significantly with BCP

content. These values were used to calculate appropriate volume percent of silica for the systems, as listed in Section 2.2.1.

Table 6. Densities of the cured neat and modified epoxy matrices.

	Epoxy	Epoxy + 2.5 phr BCP	Epoxy + 5 phr BCP
Density	1.2 g/cm^3	1.2 g/cm^3	1.19 g/cm^3

3.1.2 Filler Concentration Measurements

After finding the appropriate concentrations to formulate the various systems, it was necessary to calculate the various concentrations of fillers. In order to determine the rubber filler concentration, that was simply done following Equation 2.8 in Section 2.3.2.2. For the silica and hybrid systems, the volume percent silica in all of the systems was confirmed using TGA. The resultant nominal and determined volume percents can be seen below in Table 7.

It should be noted that the silica volume percents are an average of two measurements. These two measurements were determined to be within ±0.5% from the nominal value. Through this small deviation from the nominal value, it was concluded that there was no settling of the silica in the samples.

3.1.3 Glass Transition Temperature (T_g) Measurements

The glass transition temperatures, T_g, for all of the systems can be seen in Figure 13. Note that the addition of filler has a minimal effect on the glass transition temperature. There is a slight increase in the T_g with the addition of fillers, however there is a minimal effect from the filler type and concentration. The dashed line on the graph represents the value of T_g for the neat resin. Additionally, to clarify the hybrid systems, the various designations have been noted in Figure 13. The filler content that is noted for each of the hybrid systems are the total content of the silica and hybrid, as noted below in Table 7.

Table 7. Calculated and measured filler contents.

Type	System	Rubber Content		Silica Content		Total Content (vol%)
		Nominal Value (phr)	Calculated Value (vol%)	Nominal Value (vol%)	Measured Value (vol%)	
BCP	**2.5 phr**	2.5	1.1	0	-	1.1
	5 phr	5	2.2	0	-	2.2
	7.5 phr	7.5	3.2	0	-	3.2
	10 phr	10	4.2	0	-	4.2
Silica	**10 vol%**	0	-	10	10.0	10.0
	15 vol%	0	-	15	14.6	14.6
	20 vol%	0	-	20	20.6	20.6
	30 vol%	0	-	30	29.8	29.8
Hybrid	**2.5 phr/20 vol%**	2.5	0.9	20	19.8	20.7
	2.5 phr/30 vol%	2.5	0.8	30	30.7	31.5
	5 phr/ 20 vol%	5	1.8	20	19.4	21.2
	5 phr/30 vol%	5	1.6	30	30.1	31.7

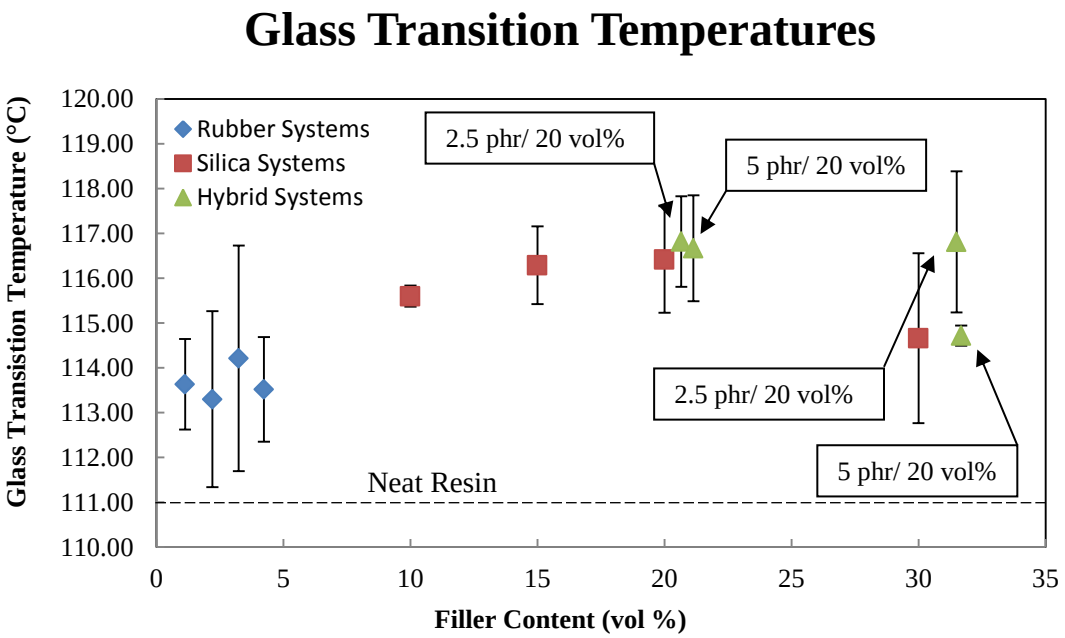

Figure 13. Glass transition temperature for the various systems as a function of volume percent filler. Note that the dashed line represents the T_g of the neat resin.

3.1.4 Coefficient of Thermal Expansion (CTE) Measurements

The linear coefficients of thermal expansion were found for all of the systems, both below and above the glass transition temperature. The results for the glassy CTE and the rubbery CTE can be seen in Figures 14 and 15, respectively. The dashed line indicates the CTE for the neat epoxy systems.

From these plots it can be seen that, below T_g, increasing amount of rubber increase the CTE and increasing amounts of silica decrease the CTE. Interestingly, there seems to be a minimal increase with the addition of rubber into the hybrid systems, indicating that the silica content controls this property. Above T_g, the rubber plays a minimal effect on the CTE, since the epoxy matrix is rubbery at these temperatures, and the increasing amounts of silica again decrease the CTE.

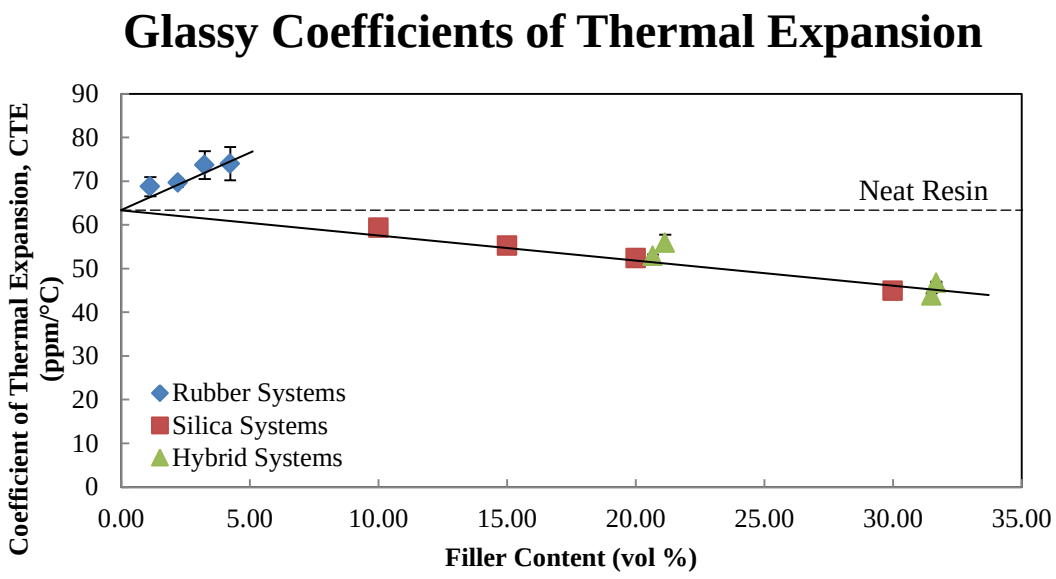

Figure 14. Coefficient of thermal expansion below T_g for all the systems. Note that the dashed line indicates the Glassy CTE for the neat resin.

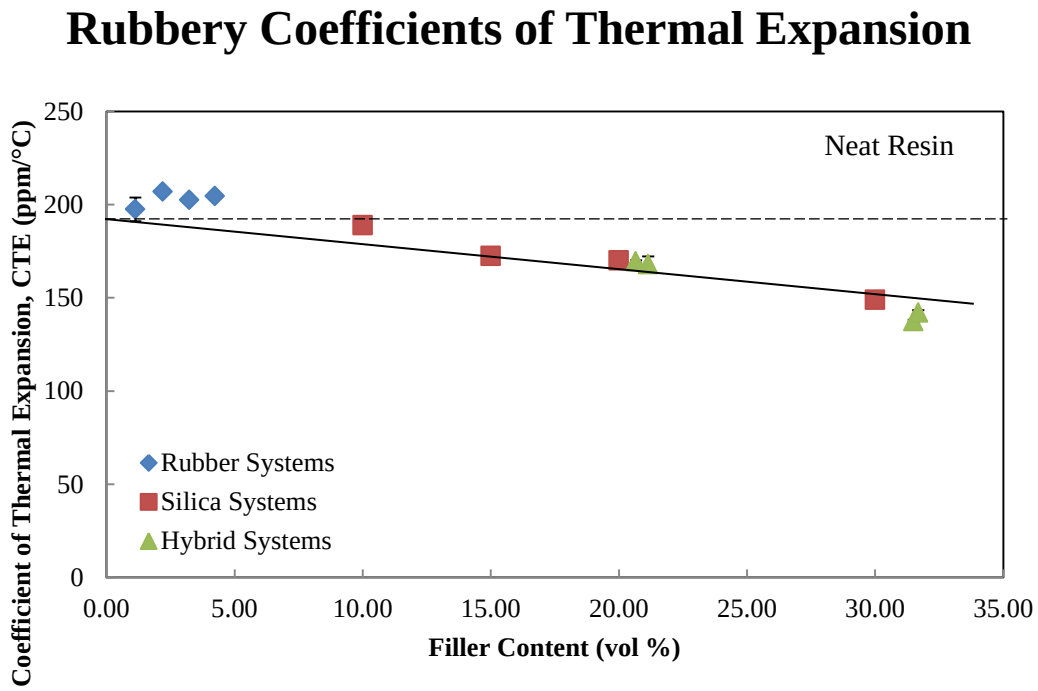

Figure 15. Coefficient of thermal expansion above T_g for all the systems. Note that the dashed line indicates the Rubbery CTE for the neat resin.

3.1.5 Compressive Yield Strength (σ_y) Measurements

The results from the compressive yield strength measurements can be seen below in Figure 16. It can be seen that the addition of rubber decreased the yield strength, while the addition of silica leads to an increase. It should also be noted that the addition of rubber in the hybrid systems seems to have a more significant effect on the compressive yield strength than it did on the CTE. The addition of the rubber in the hybrid systems decreased the yield strength by around two times the value it decreased the yield strength of the neat resin.

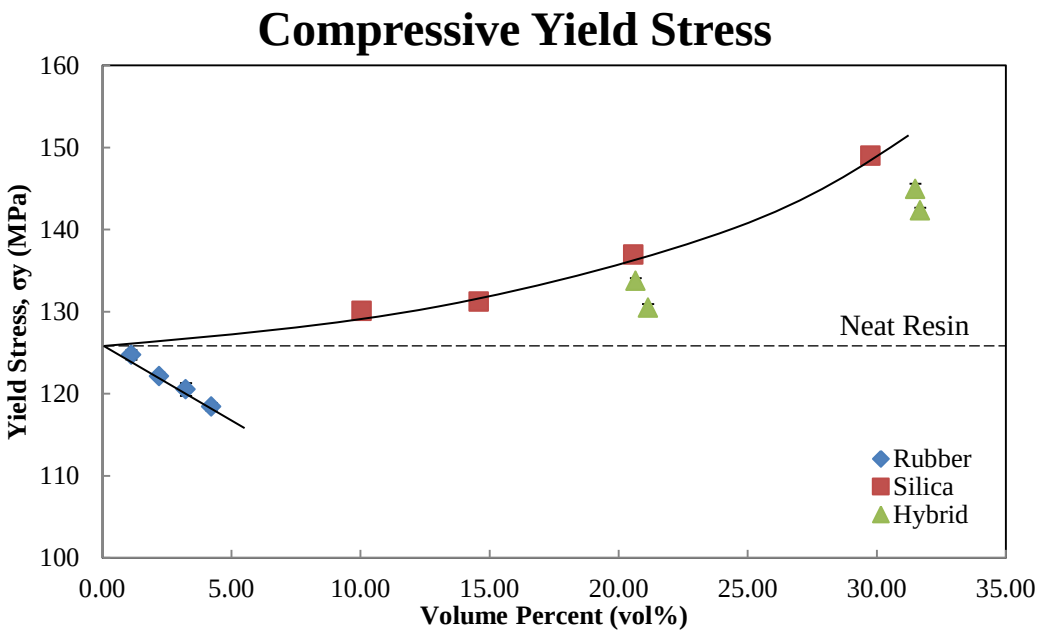

Figure 16. Compressive yield stresses for all of the systems. Note that the dashed line indicates the compressive yield stress for the neat resin.

3.1.6 Fracture Toughness (K_{IC}) Measurements

The value of the stress intensity factor, K_{IC}, was measured and the results can be seen in Figure 17. When compared to the neat resin, all of the systems exhibited higher fracture toughness. Due to the nano-sized nature of the rubber, it is possible to see vast increases in the fracture toughness with only a small addition. However, in the presence of silica, in the hybrid systems, these large increases that were noted with the small filler content in the BCP only system are not noted. Figure 18 shows the hybrid systems plotted in terms of the amount of silica the system contains. The lines in the graph shows the trends for the 0, 20 and 30 vol% silica systems. It can be seen with these lines that with the addition of BCP, there is an increase from that systems silica content with 0 vol% rubber. With the hybrid systems, however, the rubber is able to impart less toughness than in the epoxy/BCP system, which can be determined from the lower slope in the hybrid systems.

This figure also shows how the formation of the hybrid system creates a material with a higher fracture toughness that the particles added separately.

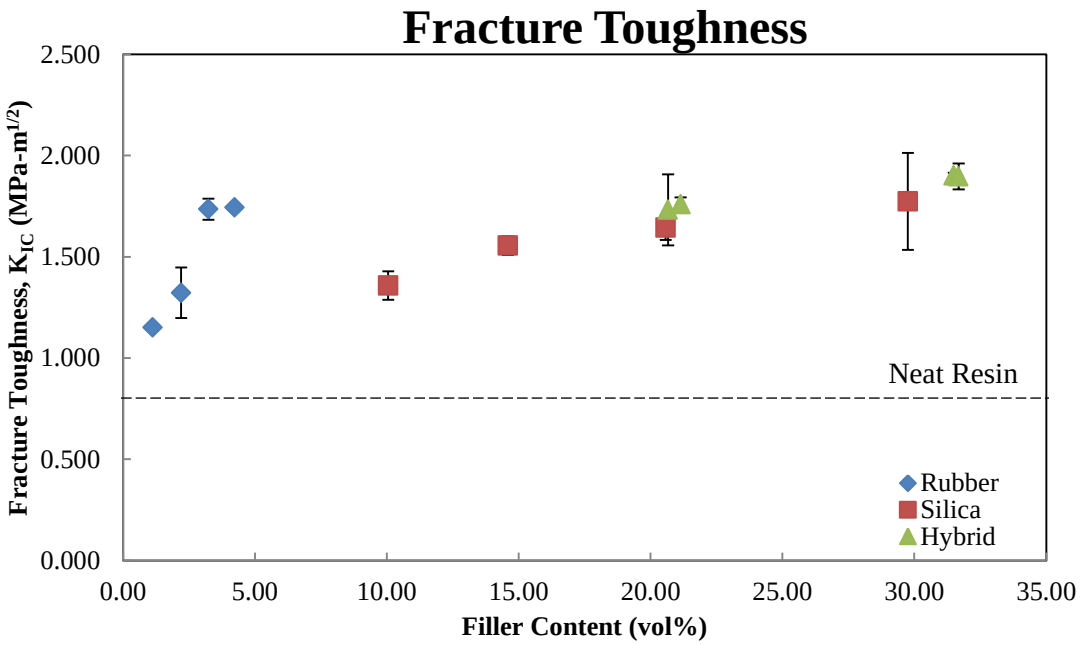

Figure 17. Fracture toughness of all of the systems. Note that the dashed line indicates the fracture toughness for the neat resin.

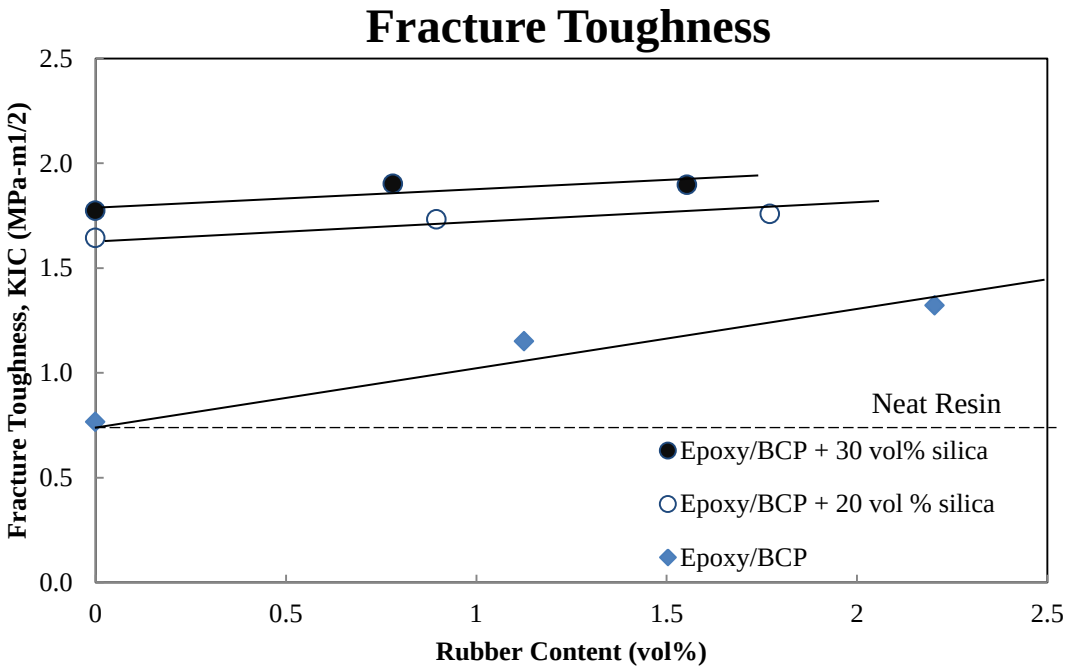

Figure 18. Fracture toughness of the hybrid systems with the silica and rubber only systems for comparison. Note that these are graphed in terms on rubber content.

3.1.7 Fracture Surface Imaging

The fracture surfaces were imaged using SEM. In Figure 19, the surface textures of the rubber-toughened epoxy systems are portrayed at high magnification. Figure 20 shows an example of the stress whitened regions for the BCP systems at low magnification. This example was taken from the 7.5 phr system. Comparable images, although with stress whitened regions of different lengths, were seen in each of the rubber systems. Rubber particle cavitation was expected in these systems, since the main mechanism for rubber-toughening involves rubber particle cavitation followed by matrix shear banding. It was, therefore, surprising that cavitation was not observed, even at this scale, and this surface texture is instead noted.

The stress whitened regions of the silica systems can be seen in Figure 21. The images on the left are at low magnification and the images on the right are high magnification. It can be seen in the images at the lower magnification that the size of the stress whitened zone increases with the addition of the silica particles. In the images at the higher magnification, the debonding of the silica particles from the matrix can be seen. Figure 22 depicts the fast fracture region of these systems. It can be seen that, in the fast fracture regime, the particles are still incorporated in the matrix and have not debonded.

Another note that should be taken from these images in Figure 22 is that there is a range in the size of the silica particles. The MSDS for the silica particles notes a size distribution within the range of 2 to 10 μm. This range seems to be comparable to the particles seen in the micrographs.

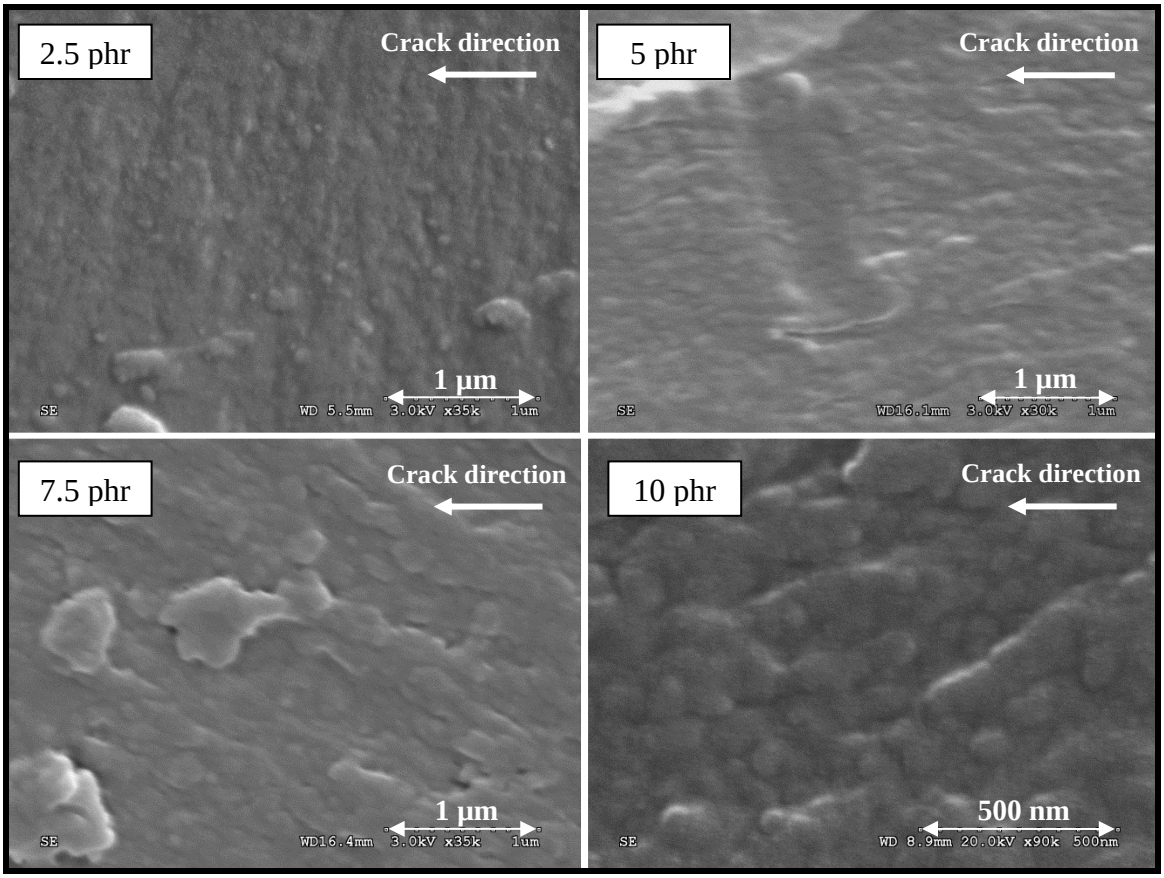

Figure 19. Fracture surfaces of the stress whitened regions of the rubber only systems. The cracks propagated from right to left.

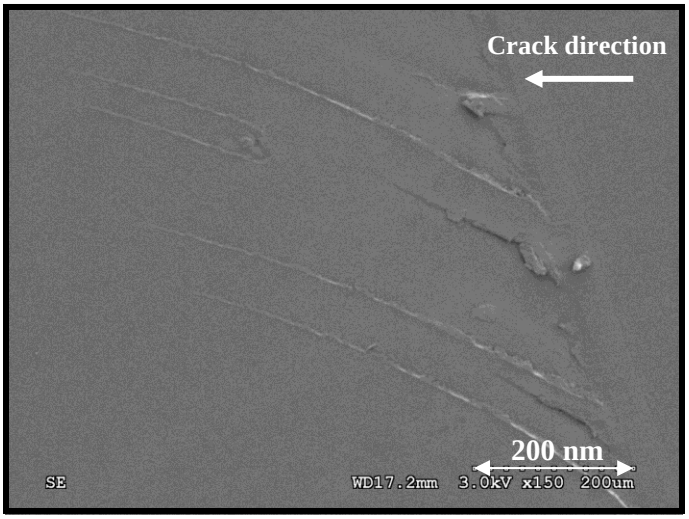

Figure 20. Image of the entire stress whitened region at low magnification of the 7.5 phr BCP system.

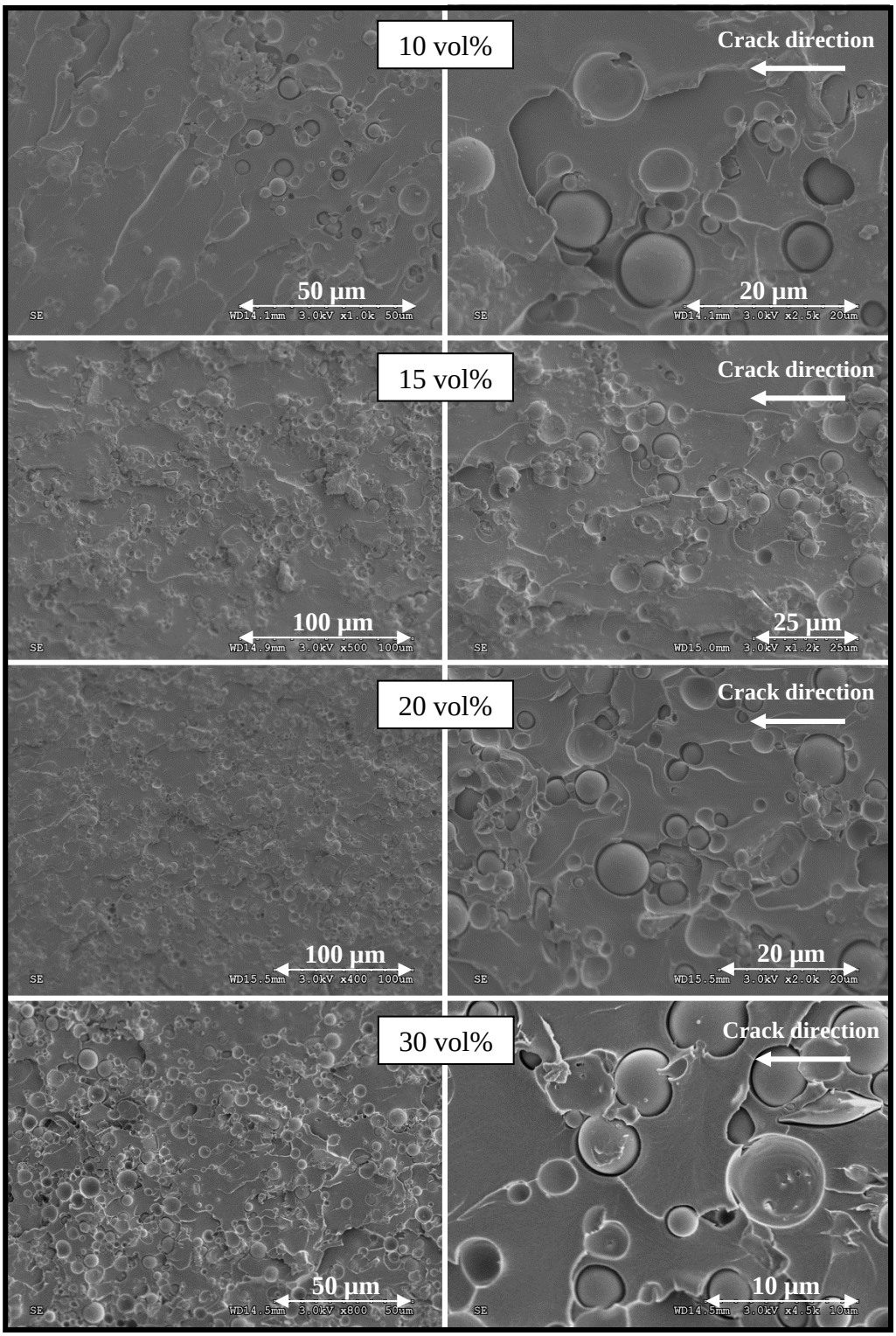

Figure 21. Fracture surfaces of the stress whitened regions of the silica only systems. The cracks propagated from right to left.

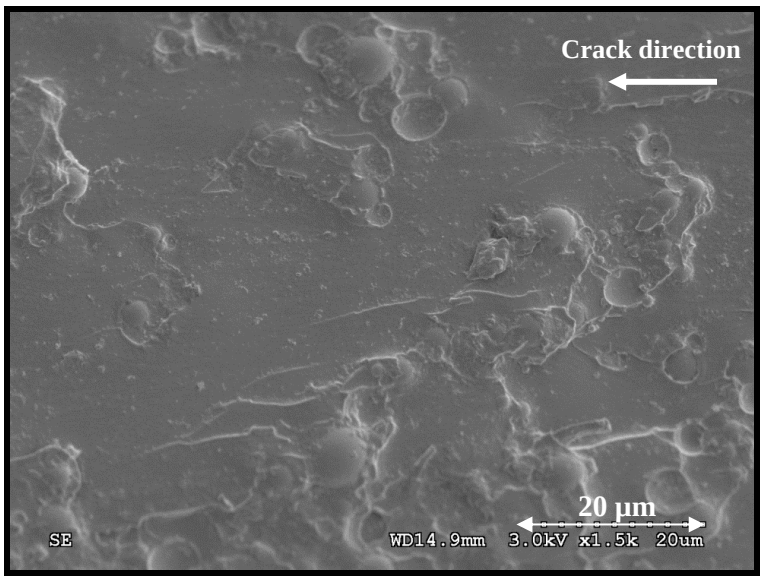

Figure 22. Image of the fast fracture region of the silica only systems. This image was taken from the 15 vol% silica system.

The fracture surfaces of the hybrid systems can be seen in Figure 23. The images on the left show a lower magnification to show the deformation around the silica particles, while the images on the right show a higher magnification to show the deformation of the rubber nanoparticles. It can be seen in the lower magnification that the silica particles debonded, similar to the silica only systems. The images at a higher magnification show that there is cavitation of the rubber particles that was not seen in the rubber only systems, potentially due to the triaxial stresses provided by the larger silica particles, as seen by Dittanet [58]. Additionally, Figure 24 shows images at low and high magnification of the fast fracture region of the 2.5 phr BCP/20 vol% silica hybrid system. It can be seen that the silica particles are incorporated in the matrix, however, the rubber has continued to cavitate. Finally, Figure 25 shows the interior of one of the fully debonded silica particles in the stress whitened zone of the 5 phr BCP/20 vol% silica system. It can be seen in this image that the addition of rubber changed the interaction between the silica particle and

the matrix, possible preventing debonding and promoting crack pinning and bridging, as has been seen by Azimi et al. [40].

This effect of large particles changing the small particles interaction with the matrix in hybrid systems has been seen a various other studies [40, 56-58]. In all of these papers, whether the systems were toughened with silica, rubber, or a combination of the two, the large particles are seen to produce a stress concentration in the matrix. This stress concentration then serves to cavitate or debond the smaller particles and leads to matrix void growth. The deformation of these small particles then lowers the driving force for the large particles to debond by relieving the hydrostatic pressure in the matrix [40, 56]. As mentioned, these results align with what was seen in the current study.

From the discussion above it can be summarized that, from these SEM micrographs, the BCP only systems do not seem to be toughened through cavitation. This result is unexpected and needs to be further investigated in order to confirm the validity of this statement. In the silica systems, there was debonding of the silica particle from the matrix and subsequent void growth surrounding the particle. In the hybrid systems, there was a shift in the toughening mechanism that were present. There was still particle debonding and matrix void growth of the silica particles; however, additionally there was cavitation of the rubber particles throughout the entire fracture surface.

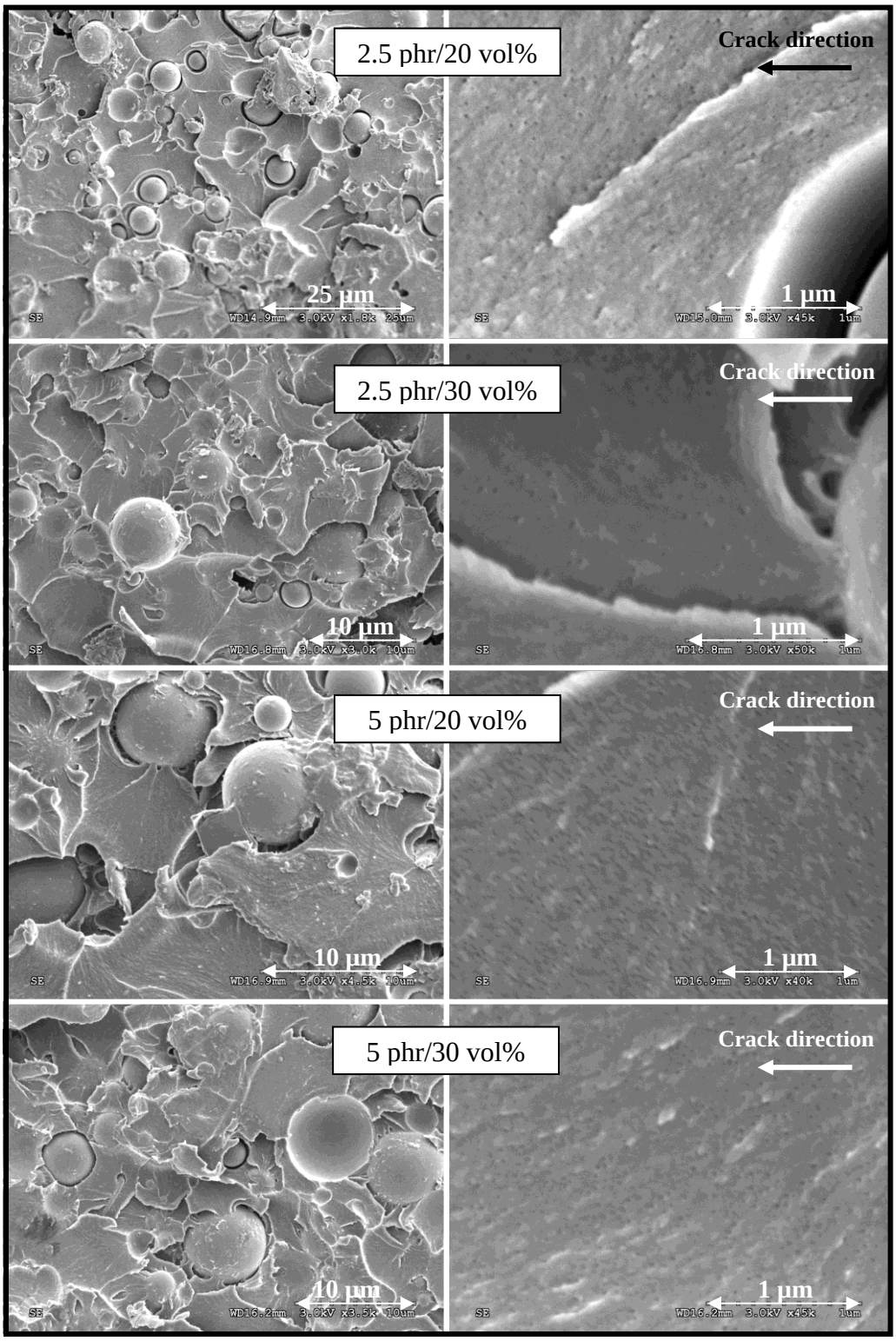

Figure 23. Fracture surfaces of the stress whitened regions of the hybrid systems. The cracks propagated from right to left.

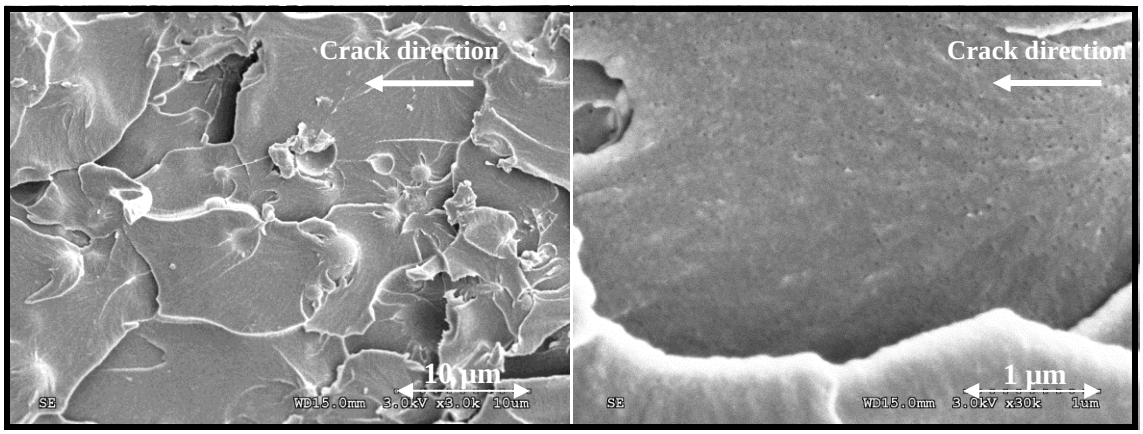

Figure 24. Fast fracture region of the 2.5 phr BCP/20 vol % silica hybrid system at low and high magnification.

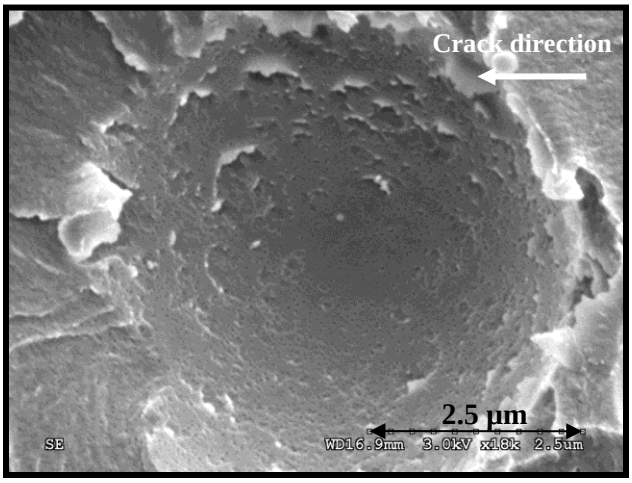

Figure 25. High magnification image of the interior of a debonded silica particle in the 5 phr BCP/20 vol% silica hybrid system.

3.1.8 Plastic Zone Imaging

In order to further investigate the toughening mechanisms, the plastic zone size was investigated through transmission optical microscopy (TOM). An example of the bright field and cross polarized images can be seen in Figure 26. These images come from the 10 phr sample. Figures 27, 28, and 29 depict the cross polarized images from the BCP only, silica only, and hybrid systems, respectively. In the cross polarized images, the area that is bright is due to the birefringent nature of the shear bands and plastic deformation

present. It should be noted that the sample is on the bottom half of the image and the line in the middle of the image is the fracture surface of the system.

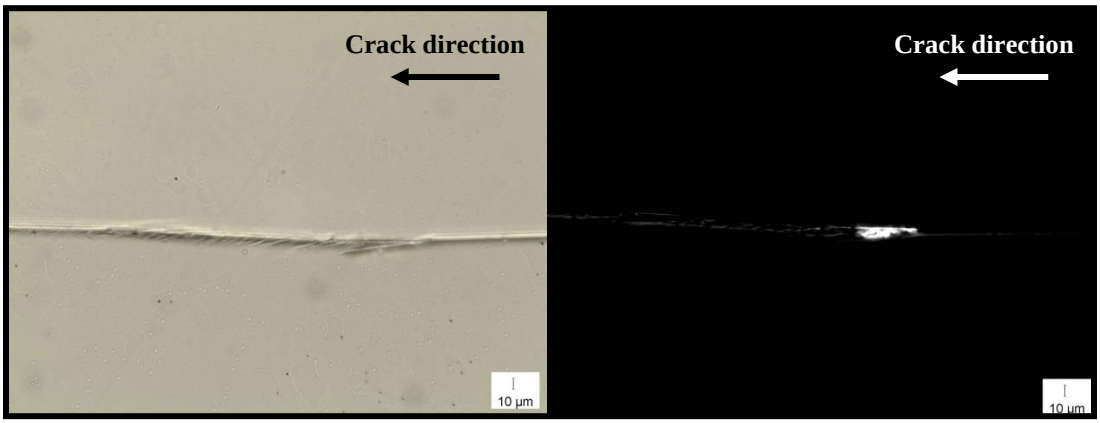

Figure 26. Bright field (left) and cross polarized (right) images from the 10 phr sample. Note that the crack propagates from right to left.

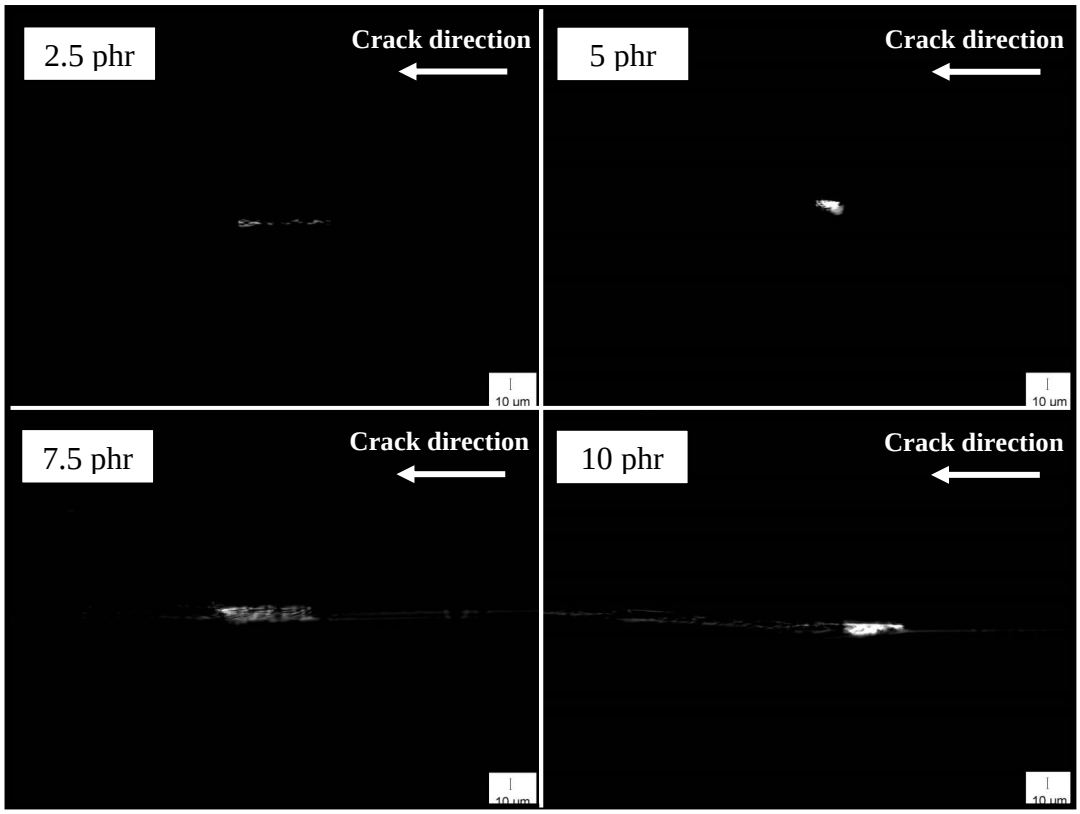

Figure 27. Cross polarized images from the BCP only systems.

In Figure 27, the cross polarized images from each of the BCP only systems can be seen. It can be noted that the size of the plastic zone increases with increasing rubber

content. This trend of increasing plastic zone size with increasing rubber content is well documented [16, 52]. The presence of this plastic deformation is thought to indicate that the toughening mechanism present is particle cavitation and matrix void growth and shear banding [13]. Due to the lack of cavitation seen in the SEM micrographs, it is interesting to note that increasing rubber particle content still leads to an increased plastic zone size, indicating that there is a formation of shear bands due to the rubber particles.

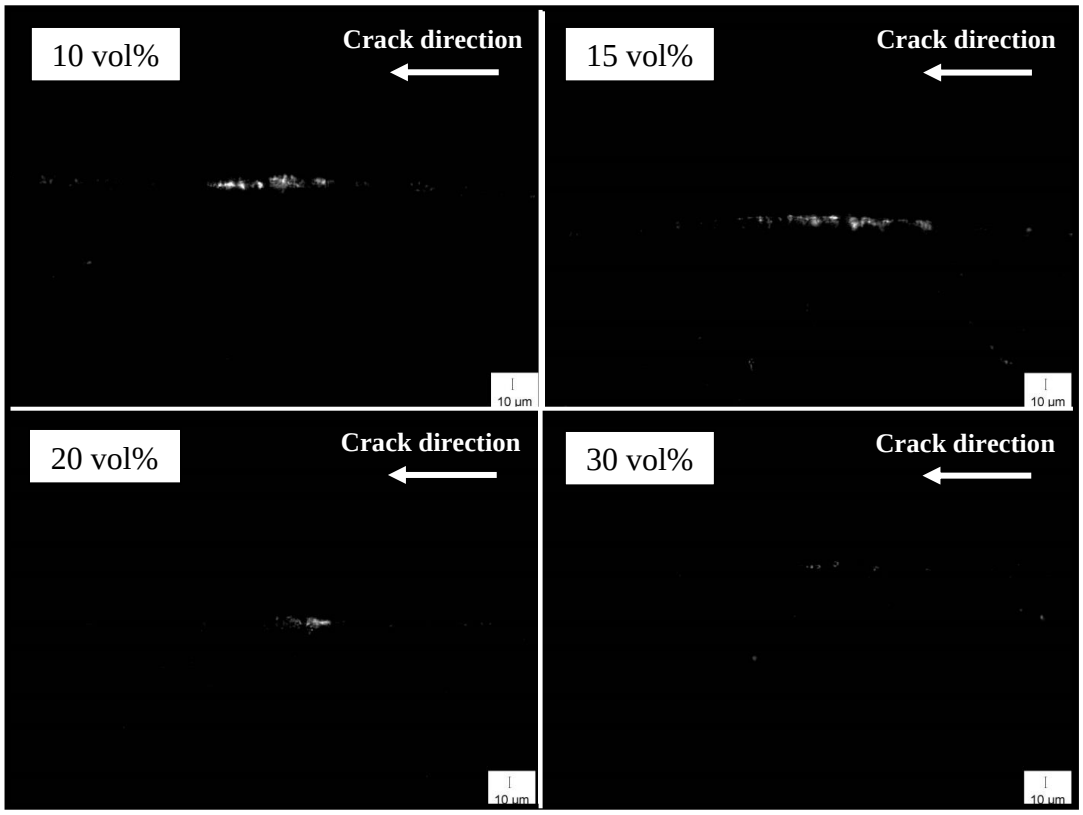

Figure 28. Cross polarized images from the silica only systems.

Figure 28 shows the cross polarized images from the silica only systems. In these systems it can be seen that the size of the plastic zone decreases with the increasing silica content. It has been noted that in epoxy systems toughened with inorganic particles, there is a presence of micro shear bands at the crack tip [34]. This birefringent region which indicates the plastic zone caused from the micro shear bands is seen to decrease with the

addition of the micron-sized silica particles. This seems to indicate that the increasing amount of silica decreases the ability of the particles to plastically deform the matrix.

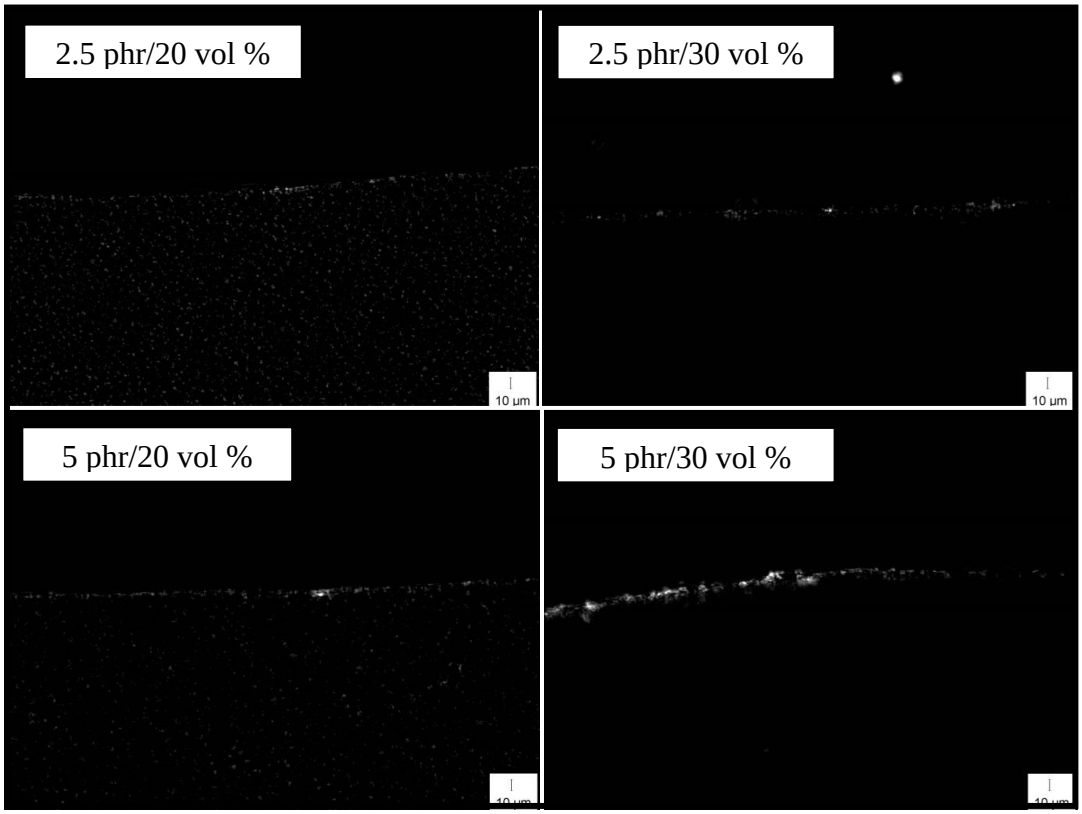

Figure 29. Cross polarized images from the hybrid systems.

In Figure 29 the cross polarized images from the hybrid systems can be seen. It is difficult to observe a trend for these hybrid systems as the plastic zone is noted as very small for every loading. In a previous study of hybrid epoxy systems toughened with micron-sized silica and nano-sized rubber, the largest fracture toughness was noted for the system with the largest plastic zone [16]. This can also be seen in this study, as the 5 phr BCP/30 vol% silica had the highest fracture toughness, however, a trend cannot be concluded from this sole fact.

From these images, a plastic zone size was measured for each of the systems. This value was then compared with the Irwin's plastic zone model, a model for predicting the

size of the plastic zone based on linear elastic fracture mechanics. Equation 3.1 summarizes Irwin's plastic zone, where r_p is the radius of the plastic zone [50]. For this calculation it was assumed that the tensile yield strength was 0.7 times the compressive yield strength and that the measurements for K_{IC} are in the plane strain regime. Additionally, the resulting comparison of the theoretical and measured plastic zones can be seen in Figure 30.

$$r_y = \frac{1}{6\pi}\left(\frac{K_{IC}}{\sigma_y}\right)^2 \qquad \textbf{(3.1)}$$

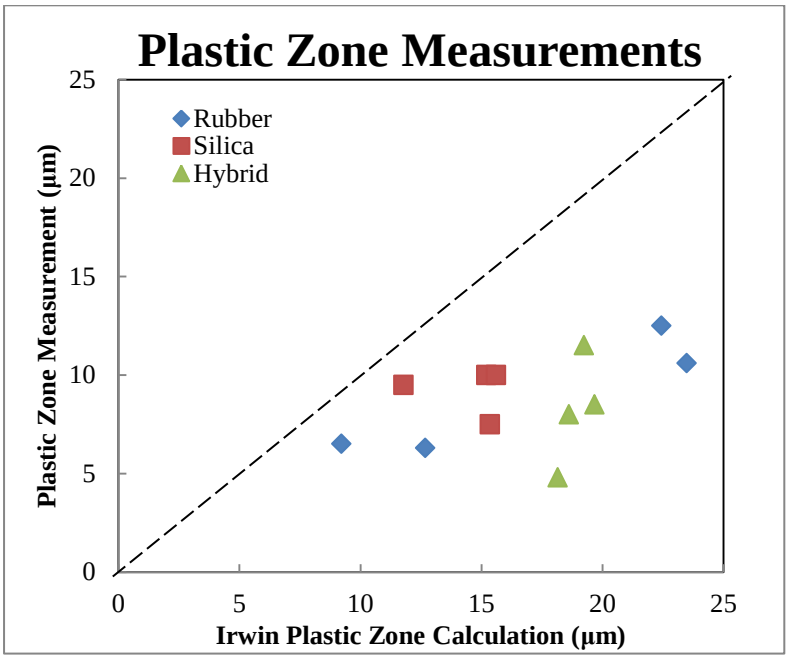

Figure 30. Comparison of Irwin's theoretical plastic zone size and the measured plastic zone size. Note that the dashed line would be an ideal 1:1 match between the Irwin plastic zone and the measured plastic zone.

It can be seen in Figure 30 that the Irwin plastic zone overestimates the measured size of the plastic zones for these systems. This can be seen in the fact that the points fall below the dashed line, which indicates a perfect correlation between the plastic zone size predicted by Irwin's calculation and the measured values. From analyzing the graph, it seems that the Irwin plastic zone overestimates the size of the plastic zone by as much as

double for some of the systems. Additionally, it calculated that the plastic zones would all be close to 19 µm for the hybrid systems, where as in reality it was seen that there was a variation in plastic zone sizes between 5 to 10 µm for the hybrid systems.

3.2 Discussion

3.2.1 Glass Transition Temperature (T_g)

The T_g found for the neat resin was comparable to that found for the mole ratios of 0.4 aniline to 0.6 mPDA by Crawford and Lesser [9]. They found this Tg to be 114.8°C. Similarly, Davies found a slightly higher Tg for the neat resin [16]. The value that he determined to be the T_g was 116.5°C. If it is assumed that the pure epoxy resin T_g in this study was determined to be a couple degrees Celsius lower, it can be seen more clearly that there is not a significant effect of the addition of particles on the resultant T_g. The addition of rubber leads to a slight decrease in the T_g, but the silica and hybrid systems do not affect this property. This result can be seen clearly in Figure 31 below which depicts the T_g data with the adjusted T_g, using the T_g found from Davies data.

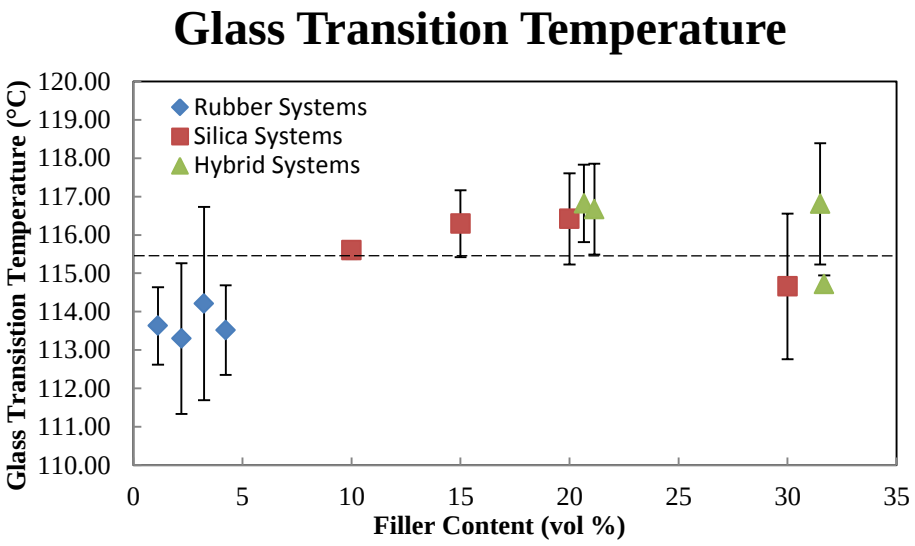

Figure 31. Glass transition temperature for the various systems as a function of volume percent filler. Note that the dashed line represents the adjusted T_g of the neat resin [16].

3.2.2 Coefficient of Thermal Expansion (CTE)

The CTE can be predicted through the use of a rule of mixtures model. This model can be seen stated below in Equation 3.2. In this equation α is the CTE and V is the volume fraction. The subscripts c, f, and m indicate the composite, filler, and matrix, respectively. For the use of this model, the CTE for the silica particles was taken to be 5.1 ppm/°C as is listed on the MSDS for the particles used in this study. For the neat resin, the CTE was determined in the study to be 65.3 ppm/°C. The CTE of the PBA phase of the rubbery particles was taken to be 200 ppm/°C. This was assumed due to the fact that in the rubbery regime, the CTE of the rubber only systems remained comparable to the neat resin at 200 ppm/°C and did not vary with concentration.

$$\alpha_c = V_f \alpha_f + V_m \alpha_m \qquad \textbf{(3.2)}$$

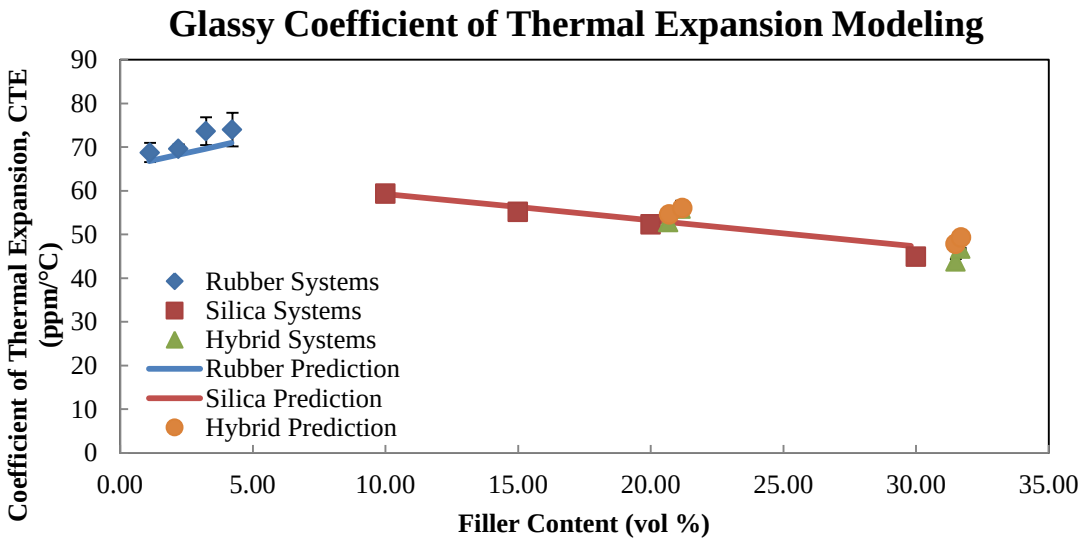

Figure 32. Modeling of the glassy coefficient of thermal expansion.

The results of the rule of mixtures can be seen above in Figure 32. It can be noted that this model was able to predict what was seen in the various systems. It can therefore

be assumed that the CTE follows a rule of mixtures modeling and various other concentrations of these fillers could be predicted for these hybrid systems.

3.2.3 Compressive Yield Strength (σ_y)

There are various models that can be used to predict the yield strength of composite systems [53-55]. One model that was proposed to predict the yield strength of a rubber-toughened system assumed that the particles were to be considered as voids [53]. The reason this assumption can be taken as a good estimation is due to the fact that the modulus of the particles is much lower than that of the matrix. The equation used in this model can be seen in Equation 3.3. In this equation, k is an experimental constant, f is the volume fraction, and a and b are parameters determined with the bulk and shear moduli of the epoxy matrix and the volume fraction of rubber particles, as explained by Wang et al [53]. Additionally, the subscripts c, m, and f indicate the composite, matrix, and filler, respectively.

$$\sigma_{yc} = \frac{\sigma_{ym}}{b + k * f_{f^*}{}^{a}/_{3}} \qquad \textbf{(3.3)}$$

In order to use this model there were various assumptions. The first assumption was that, while this model originally predicted the tensile stress, it would also depict the relationship of the composite in a compressive mode. Additionally, the plastic deformation of the particles was not accounted for. Finally, in order to use this model, there are fitting parameters which take into account the bulk and shear moduli. Wang et al determined the moduli of the various toughened systems and used an equation to predict the contributions from the matrix and the rubber particles. For the current study, the bulk and shear moduli were not determined, therefore, in order to make an estimation, the results from Wang et

al were used. The system used by Wang et al was a DGEBA epoxy system cured with piperidine and filled with core-shell rubber particles [53].

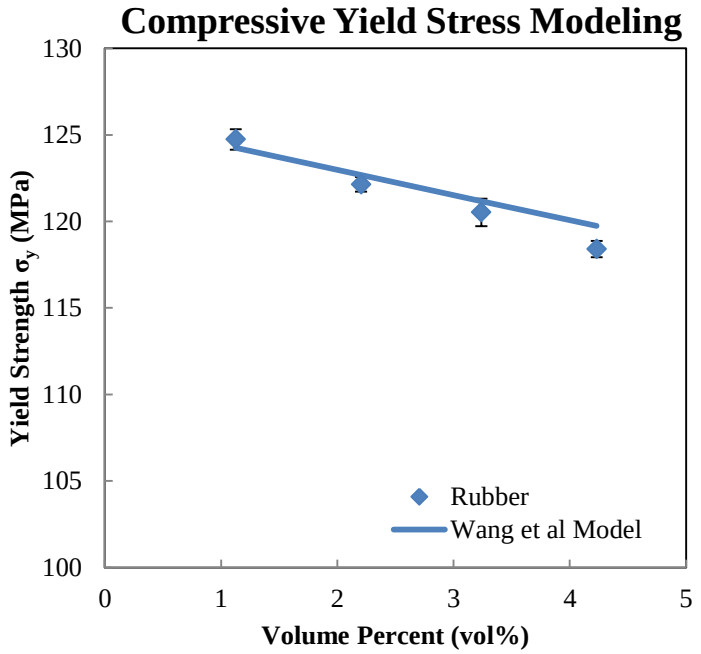

Figure 33. Modeling of the compressive yield stress of the rubber systems.

It can be seen in Figure 33 that, even with these assumptions, the modeling is relatively close. For this fit, an experimental constant, k, of 1 was used, indicating relatively close agreement. In order to see a higher agreement at the higher rubber volume percent, it would be beneficial to experimentally determine the bulk and shear moduli for this specific epoxy and rubber-toughened systems.

There are multiple ways to measure the composite yield strength of epoxy filled with inorganic particles [54, 55]. One method assumes that due to a poor interfacial bonding between the filler and the matrix, the yield strength comes solely from the effective area of the matrix [54]. When this model was applied to this system, it was not seen to have a good comparison. Due to this model's assumption that, due to poor adhesion, there is no benefit from the addition of the rigid particles, it predicted that

increasing volume percent of particles decreased the yield strength, which was not seen in this study. Another model, the Sudduth model, has a factor that accounts for the transfer of stresses between the matrix and the particles. This model can be seen in Equation 3.4 where f is the transfer efficiency parameter, ϕ is the volume fraction, and σ is the yield strength. The subscripts C, F, and M represent the composite, filler, and matrix, respectively.

$$\sigma_c = f_F \phi_F \sigma_F + \phi_M \sigma_M \qquad \textbf{(3.4)}$$

Some of the assumptions which go into this modeling are (1) that the system is below the critical pigment volume concentration, so there are no voids present and (2) that even though this model was used for tensile yield strength, it can be applied to compressive yield strength.

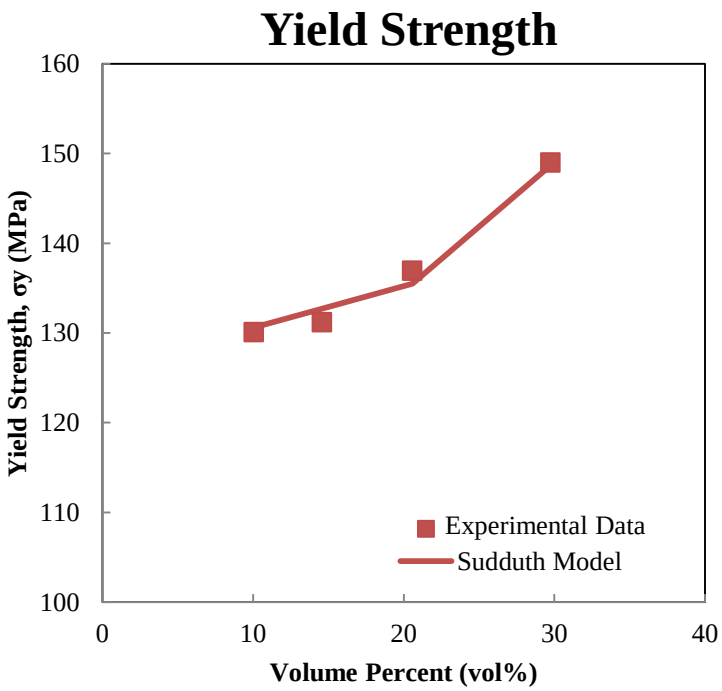

Figure 34. Modeling of the compressive yield stress of the silica systems.

Figure 34 shows the results from the application of the Sudduth model to the silica only systems. It can be seen that there is a relatively good agreement. In order to fit this model, the transfer efficiency parameter, f, of 0.0115 was used for the silica contents from 10 to 20 vol%. The value for f for 30 vol% silica was raised to 0.135. The need for this adjustment indicates that the interaction with the matrix and the particles varies with the concentration.

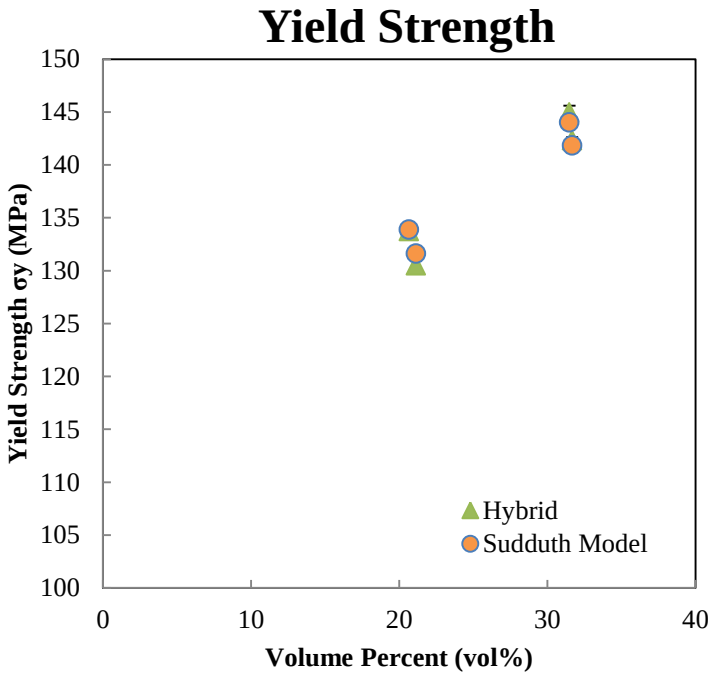

Figure 35. Modeling of the compressive yield strength of the hybrid systems.

Figure 35 shows the application of the Sudduth model to the hybrid systems. For these systems the "matrix" was taken as the rubber-toughened system which was then additionally toughened with the inclusion of silica. In order to fit these points, two values of f were used. For the systems containing 20 vol% silica, f=0.0114 and for the systems containing 30 vol% silica, f=0.0125. Both of these values were lower than the transfer efficiency parameter used in the silica only systems, indicating that the addition of rubber further affects the relationship between the particles and the matrix.

3.2.4 Fracture Toughness (K_{IC})

When compared to another system which used nano-sized rubber and micron-sized silica, the synergistic effect is comparable. Figure 36 below shows the results of fracture toughness found by Davies [16] in a system toughened with micron glass spheres and nano-sized core-shell rubber particles. The addition of these rubber particles was able to show a higher increase in fracture toughness than the BCPs in the current study, however, this could be due to the higher concentration of rubber. The addition of glass was less efficient at providing toughness than the silica spheres in the current study. The hybrid system showed the most beneficial toughening at a lower content of glass and a higher content of rubber.

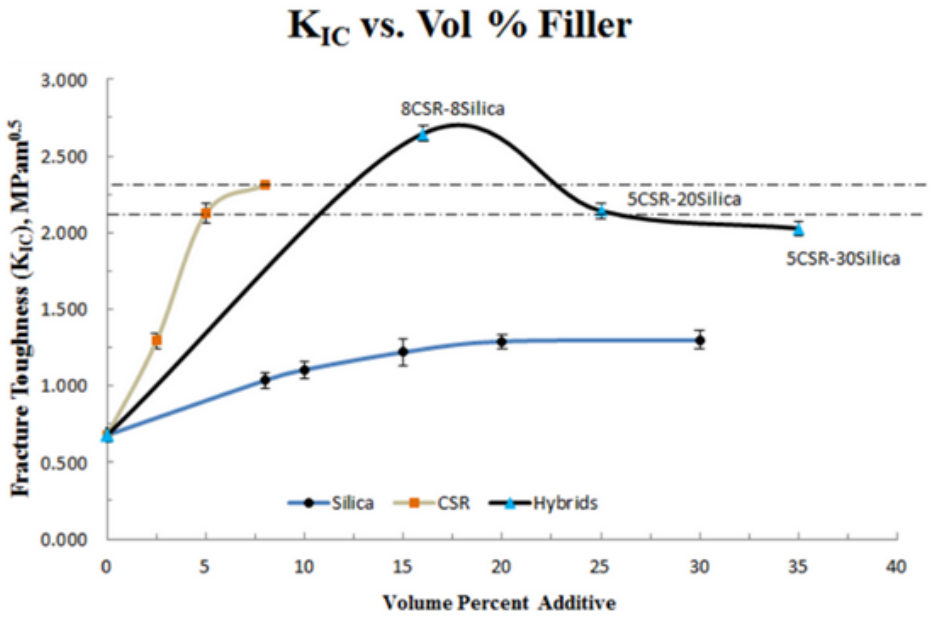

Figure 36. Fracture toughness for core-shell rubber and glass sphere toughened systems, both alone and as a hybrid system [16].

Additionally, it is possible to model the fracture toughness through a variety of means. One model that was proposed was by Kitagawa et al. [51]. This model can be seen in Equation 3.5. In this equation, the subscripts c, r, g, and neat stand for composite,

rubber, silica, and neat resin, respectively. This model is based on a rule of mixtures. The comparison of this prediction and the measured fracture toughness of the hybrid system can be seen in Figure 37.

$$K_c = K_r + K_g + K_{neat} \qquad \textbf{(3.5)}$$

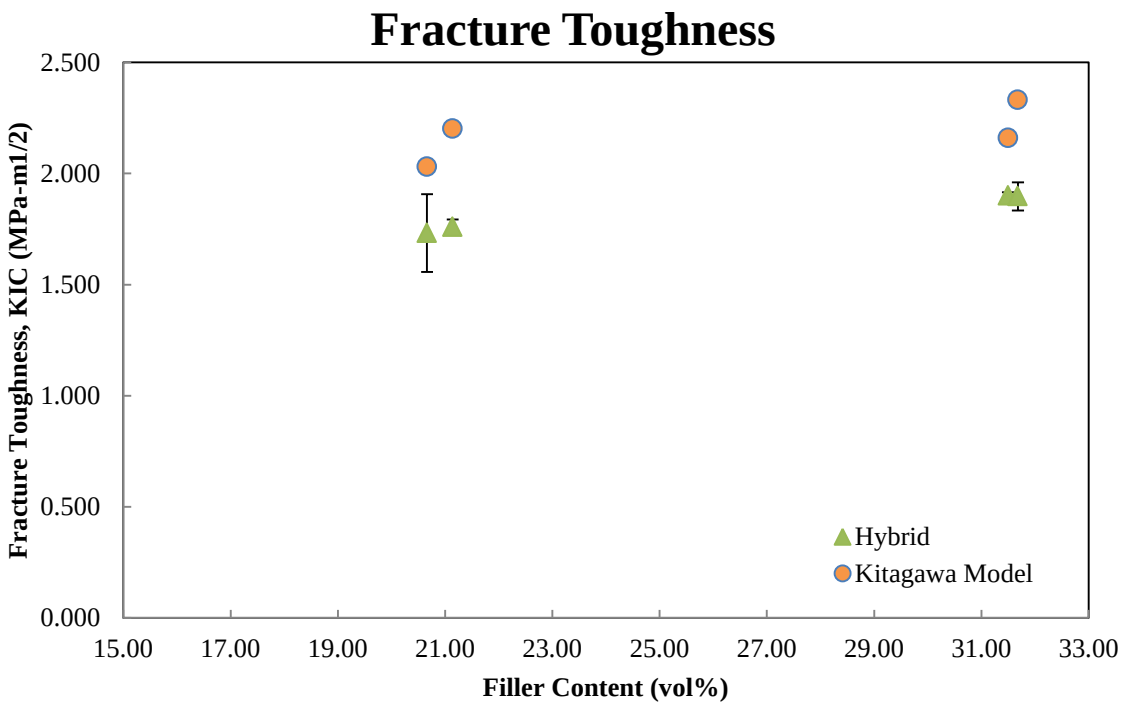

Figure 37. Comparison of the Kitagawa model to the measured fracture toughness for the hybrid systems.

It can be seen in Figure 37 that this model, which employs an additive contribution from the various components, overestimates all of the hybrid systems. This overestimation could be due to the shift in the particle interactions in the system, as this model does not take into account the particle interactions in the hybrid system. It was seen in the SEM micrographs that there was an effect in the hybrid system on both the silica and rubber particles. In these systems, the addition of the silica served to cavitate the rubber particles. This fact, and the fact that with the addition of silica there was less matrix for the rubber

particles to plastically deform, leads to the thought that in the hybrid modeling the addition from the rubber particles should be less than what was seen in the rubber only systems. In order to account for this reduction in matrix that the particle sees, the model was adjusted as can be seen in Equation 3.6, where V_m is the volume fraction of the matrix.

$$K_c = V_m K_r + K_g + K_{neat} \qquad \textbf{(3.6)}$$

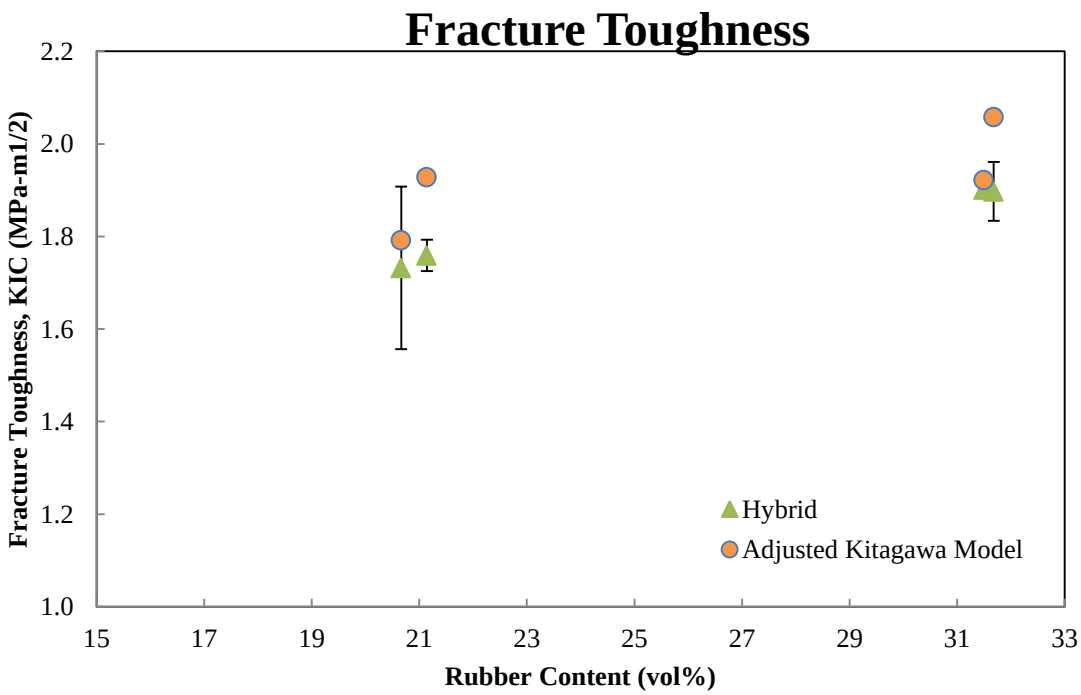

Figure 38. Comparison of the adjusted Kitagawa model to the measured fracture toughness values for the hybrid systems.

The results from this adjusted Kitagawa model can be seen in Figure 38. It can be seen that this adjustment fits the measured data much closer, indicating a better agreement when the amount of toughness the rubber particles can impart is scaled by the amount of matrix available. However, it should be noted that while that model fits better, it is still not a perfect match and deviates further from the measured fracture toughness in the 5 phr

BCP hybrid systems. This indicates that there are further interactions that need to be better documented. It can be noted from Figure 18 that the majority of the toughness in the hybrid systems seems to be imparted from the silica fillers. Therefore, even though this adjusted model lowers the impact of the rubber particles, the actual impact might be even lower. It is possible that the inclusion of silica in these hybrid systems initiates the matrix void growth and plastic deformation, close to nullifying the effect of the rubber particles.

A model that might be better able to predict the contributions from the various particles to the fracture energy (G_{IC}) can be seen below in Equation 3.7 [22, 24]. This model by Huang and Kinloch takes into account the various toughening mechanisms that are possible as a result of the toughening particles. In this equation, the subscripts ICu, s, v, and r represent the unmodified epoxy resin, localized shear banding, plastic matrix void growth, and rubber bridging. Another note for comparison between the presented results and the potential use of this model is that the fracture energy G_{IC} is related to the fracture toughness, KIC, as can be seen in Equation 3.8.

$$G_{IC} = G_{ICu} + G_s + G_v + G_r \qquad \textbf{(3.7)}$$

$$G_{IC} = \frac{K_{IC}^2}{E}(1 - \nu) \qquad \textbf{(3.8)}$$

3.2.5 Fracture Surface Imaging

There are questions that arose from the images in Section 3.1.7. Foremost among those questions is the lack of cavitation that was seen in the BCP only systems. One possible explanation was that there was a lack of morphology formed from these particles, therefore there was no distinct phase to cavitate. In order to repudiate this claim, there has been parallel work conducted in the group guided by Dr. Pearson that shows that for this BCP system there is a distinct two-phase system. Figure 39 shows transmission optical

microscopy (TEM) and atomic force microscopy (AFM) for 10 phr and 2.5 phr BCP systems, respectively. In the TEM image, the rubber second phase can be seen by the white portions of the graph. This sample was stained with osmium tetroxide, which will stain the matrix, but not the acrylate. The AFM image of the fracture surface shows a change in depth for the fracture surface. Through both of these images it can be concluded that the rubber forms a second phase in the system in a spherical morphology.

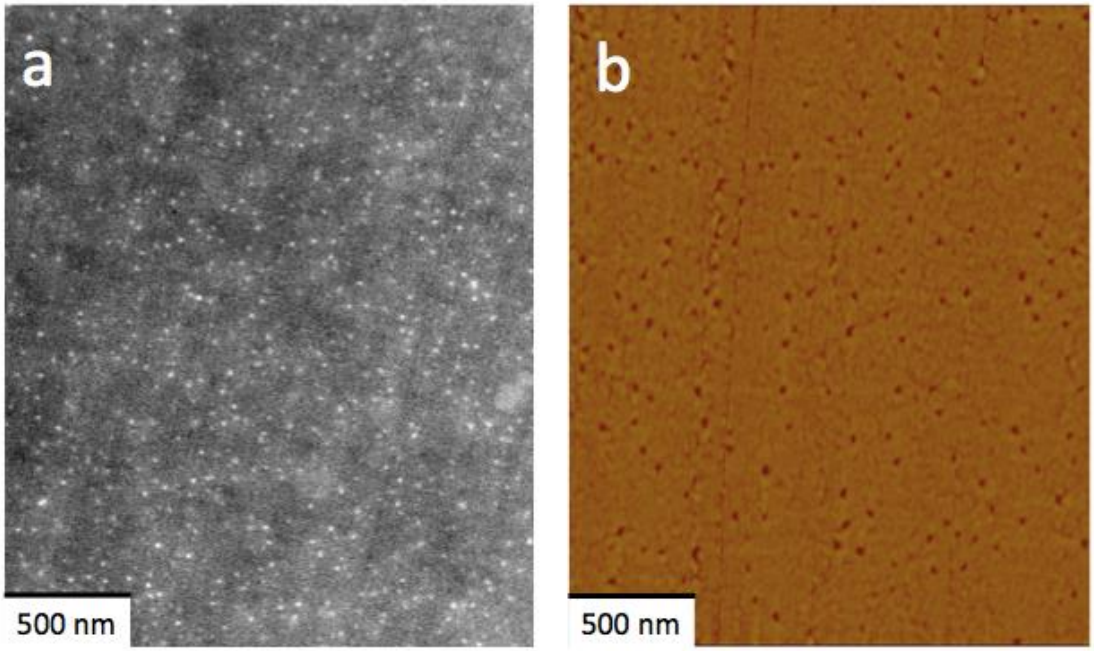

Figure 39. (a) TEM and (b) AFM images of BCP-modified epoxy showing the two-phase nature of this system (spherical micelles).

3.2.6 Plastic Zone Size

The comparison of the measured plastic zone size to the Irwin's predicted size can be seen previously in Figure 27. This figure showed a relatively good alignment between the predicted and measured plastic zone size. It is also interesting to note that the plastic zone sizes in these systems are relatively small compared to other nano-rubber- or hybrid-toughened systems. Figure 40 depicted the predicted and measured plastic zone sizes for micron-sized rubber particles [52]. It should be noted that the size of both the predicted

and measured plastic zones for these systems is on the scale of hundreds of microns, tens of times larger than the plastic zones seen in the current study. Additionally, in work conducted with slightly larger rubber particles than the particles used in this study, through still on the nano-scale, Davies noted a larger plastic zone as well [16]. The current study's presence of small plastic zones while still maintaining comparable fracture toughness indicates a higher efficiency of the particles to promote energy dissipation mechanisms.

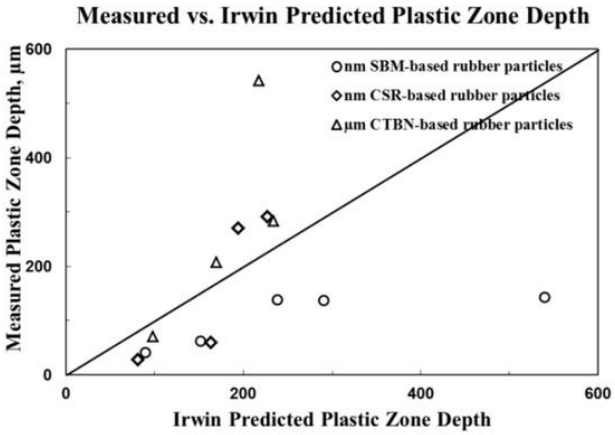

Figure 40. Comparison of Irwin's theoretical plastic zone size and the measured plastic zone size for various types and contents of micron-sized rubber particles.

3.2.7 Application of Model System

For the current study a combination of thermal and mechanical properties was of importance. Figure 41 shows the importance of these two factors, specifically fracture toughness and the coefficient of thermal expansion. This figure serves to show the benefit of the hybrid systems. For the application, a value in the top left corner is desirable. It can be seen from this graph that the addition of rubber increases the fracture toughness, but also the CTE. The addition of silica increases the fracture toughness and decreases the CTE. However, the hybrid systems take the benefit from the silica particles of a lower

CTE while providing a higher fracture toughness than either of the systems alone. It can also be noted that the addition of rubber in the 30 vol% hybrids led to a lesser increase in the CTE, while providing the highest fracture toughness of the systems.

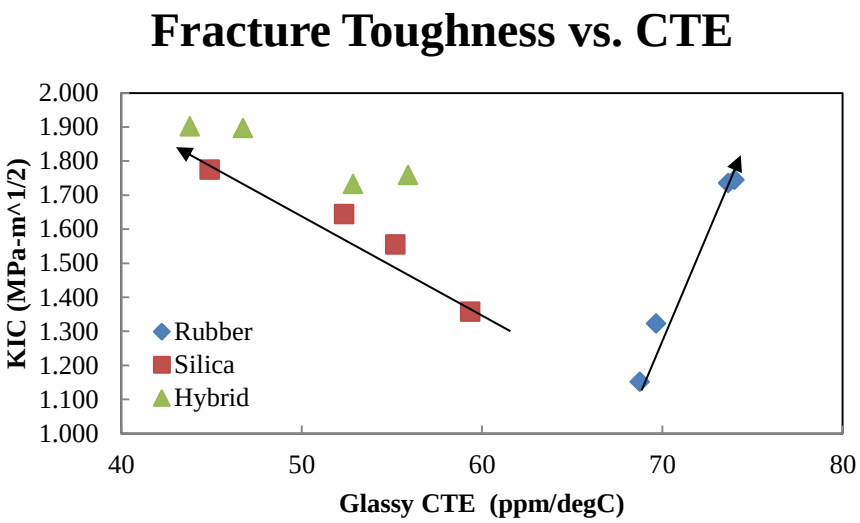

Figure 41. Fracture toughness versus CTE for each of the systems. Arrows depict the trends of increasing rubber and silica content.

While Figure 41 shows that there is a slight benefit to be taken from the hybrid systems, the increase in the fracture toughness did not achieve the level of synergism that was desired. The reason for this minimal increase could be due to the difference in the toughening mechanisms that the rubber particles proved alone as compared to in the hybrid system. It is unclear as to what sort of toughening the rubber was able to impart in the rubber only system. However, from the fracture toughness testing it is clear that there was a toughening effect as the addition of around 4 vol% rubber provided as much toughness to the matrix as 30 vol% silica. Therefore, this result should be further investigated.

4 CONCLUSIONS

For the rubber-toughened systems, an increase in the fracture toughness with BCP addition was observed. However, these increases were paired with an increase in the CTE and a decrease in the yield strength. From a study of the toughening mechanisms, it is unclear from which mechanisms dominate. A lack of cavitation was seen on the fracture surface. From the results of the TOM analysis it can be seen that the rubber plastic zone sizes are smaller than predicted by the Irwin's plastic zone calculation.

The silica-toughened systems similarly showed an increase in the fracture toughness. This increase was not offset by a loss in other mechanical properties, including CTE and yield strength. From studying the toughening mechanisms it seems as though this increase in toughness can be attributed to particle debonding and matrix void growth. The particle-matrix debonding was clearly seen in the SEM micrographs.

In an attempt to make a synergistically toughened hybrid system, these two toughening particles were combined. The result showed a minimal increase in the fracture toughness while maintaining the low CTE provided by the silica. There was a decrease in the yield strength from the silica only systems in the hybrid systems; however, it was still higher than the neat resin value. The most interesting result from this study was the analysis of the toughening mechanisms. The addition of the rubber in the hybrid system seems to promote silica particle-matrix adhesion, leading to a particle that was more difficult to debond and more likely to crack pin or bridge. Also, the addition of the silica caused the rubber particles to cavitate, likely due to the triaxial stress provided by these stiff particles.

In conclusion, a slightly tougher material was seen by the creation of a hybrid rubber silica composite. Meanwhile, the inclusion of the silica maintained the preferable mechanical properties. These results show a trend that could be optimized to create an ideal material for the application.

5 RECOMMENDATIONS FOR FUTURE WORK

5.1 Investigation of Rubber Morphology

Due to the interesting, and unexpected, results of the SEM micrograph of the rubber only systems, it is recommended to investigate the toughening mechanisms in these systems in more detail. The first step that would be recommended for this further study would be a more in-depth understanding of the morphology of the rubber particles in the rubber only and hybrid systems. It should be seen if there is a change in blend morphology between the rubber only and hybrid systems that could account for the presence of rubber particle cavitation in the hybrid systems.

5.2 Comparison between Diblock Toughened Systems

The interesting effects of the diblock copolymers should be further investigated. It would be ideal to compare this system to various other self-assembling diblock copolymers. From this comparison it could be determined if the topography of the fracture surface present in rubber-toughened systems in this study are representative of all nano-sized self-assembling diblock copolymers. Additionally, if this effect is unique to this system, it should be determined if it preferable to the other systems.

5.3 Investigation into the Effect of Mixing and Cure Schedule

Due to the difference in the fracture surfaces seen in the rubber only and hybrid systems, the question arose as to whether the presence of the silica affected the self-

assembly of the rubber particles. In order to investigate this, it would be ideal to run various samples where the silica and rubber were added at different stages of the mixing and then investigate the morphology of the rubber particles. This study would determine what the effect, if any, the inclusions of the particles in the mixing process plays on the formation of the rubber morphologies.

After this study into the effect of the mixing, the effect of the cure schedule should be investigated. If the addition of the silica particles changes the cure kinetics of the system it is also possible that this would lead to a difference in the rubber morphologies. If the silica accelerates or decelerates the reaction, the rubber would have a different amount of time to self-assemble than in the rubber only system, which could lead to the observed differences.

5.4 Further Investigation of Toughening Mechanisms

After it has been determined what the morphology of the rubber particles is, it would be easier to determine the best method to observe the toughening mechanisms they provide. For example, if the particles that self-assemble in the rubber only system are smaller than those in the hybrid system, the lack of resolution could be the reason it was not possible to see the cavitation in these systems. If this is the case, it would be possible to qualify the fracture surface through AFM at a higher resolution.

Additionally, due to the unique fracture surfaces that arose, it would be interesting to apply various models to the systems and observe if there is a model in existence, such as the Huang and Kinloch model, which matches the results and explains the contributions from each of the various toughening mechanisms.

5.5 Further Optimization of the Hybrid Systems

Finally, this study showed that the addition of rubber into a silica system created an interesting system and has the potential to create a truly superior system. In order to achieve this effect, these particles should be tested with varied concentrations of rubber and silica in order to find the optimum system.

6 REFERENCES

[1] Zhang, Z., & Wong, C. P. (2004). Recent advances in flip-chip underfill: materials, process, and reliability. *Advanced Packaging, IEEE Transactions on*, *27*(3), 515-524.

[2] Liu, X., Haque, S., Wang, J., & Lu, G. Q. (2000). Packaging of integrated power electronics modules using flip-chip technology. In *Applied Power Electronics Conference and Exposition, 2000. APEC 2000. Fifteenth Annual IEEE* (Vol. 1, pp. 290-296). IEEE.

[3] Chiang, D. (1997). Underfill material selection for flip-chip technology. M.S. Thesis. Cambridge MA: Massachusetts Institute of Technology.

[4] Prozonic, T. (2012). The effect of epoxy network structure on toughenability. M.S. Thesis. Bethlehem PA: Lehigh University.

[5] Lu, F., Kausch, H. H., Cantwell, W. J., & Fischer, M. (1996). The effect of crosslink density on the fracture toughness of core-shell modified epoxy resins. *Journal of materials science letters*, *15*(12), 1018-1021.

[6] Pearson, R. A., & Yee, A. F. (1989). Toughening mechanisms in elastomer-modified epoxies. *Journal of materials science*, *24*(7), 2571-2580.

[7] Kinloch, A. J., Finch, C. A., & Hashemi, S. (1987). Effect of segmental molecular mass between crosslinks of the matrix phase on the toughness of rubber-modified epoxies. *Polymer communications*, *28*(12), 322-325.

[8] Grillet, A. C., Galy, J., & Pascault, J. P. (1992). Influence of a two-step process and of different cure schedules on the generated morphology of a rubber-modified epoxy system based on aromatic diamines. *Polymer*, *33*(1), 34-43.

[9] Crawford, E., & Lesser, A. J. (1998). The effect of network architecture on the thermal and mechanical behavior of epoxy resins. *Journal of Polymer Science Part B: Polymer Physics*, *36*(8), 1371-1382.

[10] Lin, K. F., & Shieh, Y. D. (1998). Core-shell particles designed for toughening the epoxy resins. II. Core-shell-particle-toughened epoxy resins. *Journal of applied polymer science*, *70*(12), 2313-2322.

[11] Pearson, R. A., & Yee, A. F. (1993). Toughening mechanisms in thermoplastic-modified epoxies: 1. Modification using poly (phenylene oxide). *Polymer*, *34*(17), 3658-3670.

[12] Yee, A. F., & Pearson, R. A. (1986). Toughening mechanisms in elastomer-modified epoxies. *Journal of materials science*, *21*(7), 2462-2474.

[13] Pearson, R. A., & Yee, A. F. (1986). Toughening mechanisms in elastomer-modified epoxies. *Journal of Materials Science*, *21*(7), 2475-2488.

[14] Kody, R. S., & Lesser, A. J. (1999). Yield behavior and energy absorbing characteristics of rubber-modified epoxies subjected to biaxial stress states. *Polymer composites*, *20*(2), 250-259.

[15] Manzione, L. T., Gillham, J. K., & McPherson, C. A. (1981). Rubber-modified epoxies. II. Morphology and mechanical properties. *Journal of Applied Polymer Science*, *26*(3), 907-919.

[16] Davies, D. (2013). Fracture behavior of epoxy-based hybrid composites. M.S. Thesis. Bethlehem PA: Lehigh University.

[17] Liu, J., Thompson, Z. J., Sue, H. J., Bates, F. S., Hillmyer, M. A., Dettloff, M., ... & Pham, H. (2010). Toughening of epoxies with block copolymer micelles of wormlike morphology. *Macromolecules*, *43*(17), 7238-7243.

[18] Bacigalupo, L. (2011). Toughening of epoxies: novel self-assembling block copolymers versus traditional telechelic oligomers. M.S. Thesis. Bethlehem PA: Lehigh University.

[19] Liu, J., Sue, H. J., Thompson, Z. J., Bates, F. S., Dettloff, M., Jacob, G., ... & Pham, H. (2008). Nanocavitation in self-assembled amphiphilic block copolymer-modified epoxy. *Macromolecules*, *41*(20), 7616-7624.

[20] Kishi, H., Kunimitsu, Y., Imade, J., Oshita, S., Morishita, Y., & Asada, M. (2011). Nano-phase structures and mechanical properties of epoxy/acryl triblock copolymer alloys. *Polymer*, *52*(3), 760-768.

[21] Ruiz-Pérez, L., Royston, G. J., Fairclough, J. P. A., & Ryan, A. J. (2008). Toughening by nanostructure. *Polymer*, *49*(21), 4475-4488.

[22] Huang, Y., & Kinloch, A. J. (1992). Modelling of the toughening mechanisms in rubber-modified epoxy polymers. *Journal of materials science*, *27*(10), 2763-2769.

[23] Kunz-Douglass, S., Beaumont, P. W., & Ashby, M. F. (1980). A model for the toughness of epoxy-rubber particulate composites. *Journal of Materials Science*, *15*(5), 1109-1123.

[24] Huang, Y., & Kinloch, A. J. (1992). Modelling of the toughening mechanisms in rubber-modified epoxy polymers. *Journal of materials science*, *27*(10), 2753-2762.

[25] Dittanet, P. (2011). Fracture behavior of silica nanoparticle filled epoxy resin. PhD Dissertation. Bethlehem PA: Lehigh University.

[26] Garg, A. C., & Mai, Y. W. (1988). Failure mechanisms in toughened epoxy resins—a review. *Composites Science and Technology*, *31*(3), 179-223.

[27] Ratna, D., & Banthia, A. K. (2004). Rubber toughened epoxy. *Macromolecular research*, *12*(1), 11-21.

[28] Pearson, R. A., & Yee, A. F. (1991). Influence of particle size and particle size distribution on toughening mechanisms in rubber-modified epoxies. *Journal of Materials Science*, *26*(14), 3828-3844.

[29] Guild, F. J., Kinloch, A. J., & Taylor, A. C. (2010). Particle cavitation in rubber toughened epoxies: the role of particle size. *Journal of materials science*,*45*(14), 3882-3894.

[30] Liang, Y. L., & Pearson, R. A. (2009). Toughening mechanisms in epoxy–silica nanocomposites (ESNs). *Polymer*, *50*(20), 4895-4905.

[31] Ahmad, F. N., Jaafar, M., Palaniandy, S., & Azizli, K. A. M. (2008). Effect of particle shape of silica mineral on the properties of epoxy composites. *Composites Science and Technology*, *68*(2), 346-353.

[32] Kawaguchi, T., & Pearson, R. A. (2003). The effect of particle–matrix adhesion on the mechanical behavior of glass filled epoxies: Part 1. A study on yield behavior and cohesive strength. *Polymer*, *44*(15), 4229-4238.

[33] Kawaguchi, T., & Pearson, R. A. (2003). The effect of particle–matrix adhesion on the mechanical behavior of glass filled epoxies. Part 2. A study on fracture toughness. *Polymer*, *44*(15), 4239-4247.

[34] Lee, J., & Yee, A. F. (2001). Inorganic particle toughening I: micro-mechanical deformations in the fracture of glass bead filled epoxies. *Polymer*, *42*(2), 577-588.

[35] Hsieh, T. H., Kinloch, A. J., Masania, K., Taylor, A. C., & Sprenger, S. (2010). The mechanisms and mechanics of the toughening of epoxy polymers modified with silica nanoparticles. *Polymer*, *51*(26), 6284-6294.

[36] Dittanet, P., & Pearson, R. A. (2012). Effect of silica nanoparticle size on toughening mechanisms of filled epoxy. *Polymer*, *53*(9), 1890-1905.

[37] Bray, D. J., Dittanet, P., Guild, F. J., Kinloch, A. J., Masania, K., Pearson, R. A., & Taylor, A. C. (2013). The modelling of the toughening of epoxy polymers via silica nanoparticles: The effects of volume fraction and particle size. *Polymer*, *54*(26), 7022-7032.

[38] Zhang, H., Zhang, Z., Friedrich, K., & Eger, C. (2006). Property improvements of in situ epoxy nanocomposites with reduced interparticle distance at high nanosilica content. *Acta Materialia*, *54*(7), 1833-1842.

[39] Johnsen, B. B., Kinloch, A. J., Mohammed, R. D., Taylor, A. C., & Sprenger, S. (2007). Toughening mechanisms of nanoparticle-modified epoxy polymers. *Polymer*, *48*(2), 530-541.

[40] Azimi, H. R., Pearson, R. A., & Hertzberg, R. W. (1995). Role of crack tip shielding mechanisms in fatigue of hybrid epoxy composites containing rubber and solid glass spheres. *Journal of applied polymer science*, *58*(2), 449-463.

[41] Lee, J., & Yee, A. F. (2000). Micro-mechanical deformation mechanisms in the fracture of hybrid-particulate composites based on glass beads, rubber and epoxies. *Polymer Engineering & Science*, *40*(12), 2457-2470.

[42] Maazouz, A., Sautereau, H., & Gerard, J. F. (1993). Hybrid-particulate composites based on an epoxy matrix, a reactive rubber, and glass beads: Morphology, viscoelastic, and mechanical properties. *Journal of applied polymer science*, *50*(4), 615-626.

[43] Liang, Y. L., & Pearson, R. A. (2010). The toughening mechanism in hybrid epoxy-silica-rubber nanocomposites (HESRNs). *Polymer*, *51*(21), 4880-4890.

[44] Hsieh, T. H., Kinloch, A. J., Masania, K., Lee, J. S., Taylor, A. C., & Sprenger, S. (2010). The toughness of epoxy polymers and fibre composites modified with rubber microparticles and silica nanoparticles. *Journal of materials science*, *45*(5), 1193-1210.

[45] Kinloch, A. J., Mohammed, R. D., Taylor, A. C., Eger, C., Sprenger, S., & Egan, D. (2005). The effect of silica nano particles and rubber particles on the toughness of multiphase thermosetting epoxy polymers. *Journal of materials science*, *40*(18), 5083-5086.

[46] ASTM, E1356-08: Standard Test Method for Assignment of the Glass Transition Temperatures by Differential Scanning Calorimetry, West Conshohocken, PA.

[47] ASTM, E831-14: Standard Test Method for Linear Thermal Expansion of Solid Materials by Thermomechanical Analysis, West Conshohocken, PA.

[48] ASTM, D695-10: Standard Test Method for Compressive Properties of Rigid Plastics, West Conshohocken, PA.

[49] ASTM, D5045-99: Standard Test Methods for Plane-Strain Fracture Toughness and Strain Energy Release Rate of Plastic Materials, West Conshohocken, PA.

[50] Irwin, G. R. (1957). Analysis of stresses and strains near the end of a crack traversing a plate. *J. appl. Mech.*

[51] Kitagawa, H., Yuuki, R., & Ohira, T. (1975). Crack-morphological aspects in fracture mechanics. *Engineering Fracture Mechanics*, *7*(3), 515-529.

[52] Bacigalupo, L. (2013). Fracture Behavior of Nano-Scale Rubber-Modified Epoxies. PhD Dissertation. Bethlehem PA: Lehigh University.

[53] Wang, X., Xiao, K., Ye, L., Mai, Y. W., Wang, C. H., & Rose, L. R. (2000). Modelling mechanical properties of core–shell rubber-modified epoxies. *Acta materialia*, *48*(2), 579-586.

[54] Ahmed, S., & Jones, F. R. (1990). A review of particulate reinforcement theories for polymer composites. *Journal of Materials Science*, *25*(12), 4933-4942.

[55] Sudduth, R. D. (2006). Analysis of the maximum tensile strength of a composite with spherical particulates. *Journal of composite materials*, *40*(4), 301-331.

[56] Azimi, H. R., Pearson, R. A., & Hertzberg, R. W. (1996). Fatigue of hybrid epoxy composites: epoxies containing rubber and hollow glass spheres. *Polymer Engineering & Science*, *36*(18), 2352-2365.

[57] Pearson, R. A., & Yee, A. F. (1991). Influence of particle size and particle size distribution on toughening mechanisms in rubber-modified epoxies. *Journal of Materials Science*, *26*(14), 3828-3844.

[58] Dittanet, P., & Pearson, R. A. (2013). Effect of bimodal particle size distributions on the toughening mechanisms in silica nanoparticle filled epoxy resin. *Polymer*, *54*(7), 1832-1845.

VITA

Amelia Kyla Labak was born in June of 1990 to Janine and Stanley Labak. She attended Lehigh University for her undergraduate studies, graduating in May of 2013 with a B.S. in Materials Science and Engineering and a B.A. in Architecture. She continued at Lehigh to obtain her M.S. in Materials Science and Engineering in January of 2015 with a specialization in polymers.